Journal of Computational Physics 382 (2019) 1–26

Contents lists available at ScienceDirect

Journal of Computational Physics

www.elsevier.com/locate/jcp

Entropy stable DGSEM for nonlinear hyperbolic systems in nonconservative form with application to two-phase flows

Florent Renac

DAAA, ONERA, Université Paris Saclay, F-92322 Châtillon, France

ARTICLE INFO

Article history:
Received 23 May 2018
Received in revised form 11 December 2018
Accepted 12 December 2018
Available online 16 January 2019

Keywords:
Nonconservative hyperbolic systems
Entropy stable schemes
Discontinuous Galerkin method
Summation-by-parts
Two-phase flows

ABSTRACT

In this work, we consider the discretization of nonlinear hyperbolic systems in nonconservative form with the high-order discontinuous Galerkin spectral element method (DGSEM) based on collocation of quadrature and interpolation points (Kopriva and Gassner (2010) [39]). We present a general framework for the design of such schemes that satisfy a semi-discrete entropy inequality for a given convex entropy function at any approximation order. The framework is closely related to the one introduced for conservation laws by Fisher and Carpenter (2013) [27] and Gassner (2013) [32] and relies on the modification of the integral over discretization elements where we replace the physical fluxes by entropy conservative numerical fluxes from Castro et al. (2013) [12], while entropy stable numerical fluxes are used at element interfaces. Time discretization is performed with strong-stability preserving Runge–Kutta schemes. The present method is first validated on the Burgers and Euler equations in nonconservative form. We then use this framework for the discretization of two-phase flow systems in one space-dimension: a 2×2 system with a nonconservative product associated to a linearly-degenerate field for which the DGSEM fails to capture the physically relevant solution, and the isentropic Baer–Nunziato model. For the latter, we derive conditions on the numerical parameters of the discrete scheme to further keep positivity of the partial densities and a maximum principle on the void fractions. Numerical experiments support the conclusions of the present analysis and highlight stability and robustness of the present schemes.

© 2019 Elsevier Inc. All rights reserved.

1. Introduction

The discussion in this paper focuses on the high-order discretization of the Cauchy problem for nonlinear hyperbolic systems in nonconservative form:

$$\partial_t \mathbf{u} + \mathbf{A}(\mathbf{u})\partial_x \mathbf{u} = 0, \quad \text{in } \mathbb{R} \times (0, \infty), \tag{1a}$$

$$\mathbf{u}(\cdot, 0) = \mathbf{u}_0(\cdot), \quad \text{in } \mathbb{R}, \tag{1b}$$

where $\mathbf{u}(x, t)$ represents the vector of unknowns with values in the set of states $\Omega^a \subset \mathbb{R}^m$ and $\mathbf{A} : \Omega^a \ni \mathbf{u} \mapsto \mathbf{A}(\mathbf{u}) \in \mathbb{R}^{m \times m}$ is a smooth matrix-valued function. We assume that system (1a) is strictly hyperbolic over the set of states. If there exists a flux function $\mathbf{f} : \Omega^a \to \mathbb{R}^m$ such that $\mathbf{A}(\mathbf{u}) = \mathbf{f}'(\mathbf{u})$ for all $\mathbf{u}$ in Ω^a, (1a) can be written in conservative form for which the concept of weak solutions in the sense of distributions is used to define admissible solutions.

E-mail address: florent.renac@onera.fr.

https://doi.org/10.1016/j.jcp.2018.12.035
0021-9991/© 2019 Elsevier Inc. All rights reserved.

In the general case where $\mathbf{A}$ is not the Jacobian of a flux function, the theory of distributions does not apply which makes difficult to give a meaning to the nonconservative product $\mathbf{A}(\mathbf{u})\partial_x\mathbf{u}$ at a point of discontinuity of the solution. The work by Dal Maso, Lefloch, and Murat [20] generalizes the notion of weak solutions from conservation laws to (1) and allows to define the nonconservative product for functions of bounded variations by extending the definition by Volpert [60]. The definition is based on a family of consistent and Lipschitz paths $\boldsymbol{\phi} : [0,1]\times\Omega^a\times\Omega^a \to \Omega^a$ with bounded derivative $\partial_s\boldsymbol{\phi}(s;\cdot,\cdot)$. We refer to [20] for the complete theory and to [43, section 2] for an introduction. Across a discontinuity of speed σ, the nonconservative product $\mathbf{A}(\mathbf{u})\partial_x\mathbf{u}$ is then defined as the unique Borel measure defined by the so-called generalized Rankine–Hugoniot condition

$$\sigma[\![\mathbf{u}]\!] = \int_0^1 \mathbf{A}\big(\boldsymbol{\phi}(s;\mathbf{u}^-,\mathbf{u}^+)\big)\partial_s\boldsymbol{\phi}(s;\mathbf{u}^-,\mathbf{u}^+)ds, \tag{2}$$

where $[\![\mathbf{u}]\!] = \mathbf{u}^+ - \mathbf{u}^-$, $\mathbf{u}^-$ and $\mathbf{u}^+$ are the left and right limits of $\mathbf{u}$ across the discontinuity. Note that the notion of weak solutions now depends on the family of paths under consideration [40, Lemma 2.1].

Admissible weak solutions have to satisfy an entropy inequality

$$\partial_t\eta(\mathbf{u}) + \partial_x q(\mathbf{u}) \le 0, \tag{3}$$

for the smooth entropy-entropy flux pair (η, q) with $\eta(\cdot)$ a strictly convex function such that $\boldsymbol{\eta}'(\mathbf{u})^\top\mathbf{A}(\mathbf{u}) = \mathbf{q}'(\mathbf{u})^\top$ for all $\mathbf{u}$ in Ω^a. Many problems in science and engineering such as turbulence models, multiphase flows, shallow water flows, magnetohydrodynamics (MHD), etc. contain both conservative and nonconservative terms of the form

$$\partial_t\mathbf{u} + \partial_x\mathbf{f}(\mathbf{u}) + \mathbf{c}(\mathbf{u})\partial_x\mathbf{u} = 0, \tag{4}$$

which require different approaches for their discretizations. For smooth solutions we have $\mathbf{A} \equiv \mathbf{f}' + \mathbf{c}$ and the entropy pair satisfies $\boldsymbol{\eta}'(\mathbf{u})^\top\big(\mathbf{f}'(\mathbf{u}) + \mathbf{c}(\mathbf{u})\big) = \mathbf{q}'(\mathbf{u})^\top$ for $\mathbf{u}$ in Ω^a.

The objective of this work is to develop a general method to design arbitrary high-order schemes for (1) that satisfy the entropy inequality (3) at the semi-discrete level. We propose to use the discontinuous Galerkin spectral element method (DGSEM) based on the collocation between interpolation and quadrature points defined from Gauss–Lobatto quadrature rules [39]. Using diagonal norm summation-by-parts (SBP) operators and the entropy conservative numerical fluxes from Tadmor [55], semi-discrete entropy conservative finite-difference and spectral collocation schemes have been derived in [27,11] for nonlinear conservation laws. An energy stable DGSEM for scalar nonlinear equations has been derived in [32] using the same framework and latter an entropy stable DGSEM for the compressible Euler equations on curvilinear hexahedral meshes has been proposed in [34]. The particular form of the SBP operators allows to take into account the numerical quadrature that approximates integrals in the numerical scheme compared to other techniques that require their exact evaluation to satisfy the entropy inequality [38,35]. The work in [16] extends the DGSEM to triangular meshes and convection–diffusion equations. The DGSEM thus provides a general framework for the design of entropy conservative and entropy stable schemes for the discretization of nonlinear systems of conservation laws. Numerical experiments in [16] highlight the benefits on stability and robustness of the computations, though this not guarantees to preserve neither the entropy stability at the fully discrete level, nor positivity of the numerical solution which is necessary to define the entropy. Designs of fully discrete entropy stable and positive DGSEM have been proposed in [21,22,46,47]. A general framework for the design of entropy conservative and entropy stable schemes for steady-state conservation laws has been recently proposed in [2,3] that encompasses residual distribution schemes, discontinuous and continuous Galerkin methods with general quadrature formulas on simplex elements and flux reconstruction schemes on polygons.

Some works rely on the discontinuous Galerkin (DG) approximation of nonconservative systems of shallow water flows [33,24,56,45], MHD [41,24,10], two-phase flows [63,29,30,48,36,57,31,24], etc. Note that the works in [33] and [41] use the DGSEM as discretization method and derive, respectively, high-order entropy conservative and well balanced discretization of the shallow water equations through skew-symmetric splitting techniques, and entropy stable schemes for the ideal compressible MHD equations by using two-point numerical fluxes from [15] at element interfaces and treating the nonconservative product as source terms without particular treatment. Though not exhaustive, we also refer to the works in [5,23,25,26,58] and references therein as alternative techniques for high-order approximations of two-phase flows.

Here, we extend the works in [27,11,32,16] to nonconservative products by using the two-point entropy conservative numerical fluxes in fluctuation form introduced in [12]. This extension is clarified through the direct link between fluctuation fluxes and conservative fluxes in the case of conservation laws. One difficulty in the design of an entropy stable DGSEM lies in the treatment of the integrals over discretization elements which contain space derivatives of test functions whose sign cannot be controlled. The use of entropy conservative numerical fluxes in those integrals allows however to remove their contribution to the global entropy production in the element. The properties of high-order accuracy and approximation of the cell averaged numerical solution are also difficult to derive due to the specific form of the fluctuation fluxes. Indeed, the consistency condition has less physical meaning for fluctuation fluxes compared to conservation fluxes which require homogeneity properties in closed form. Moreover, even in the case of path-conservative fluxes [43] they require a priori

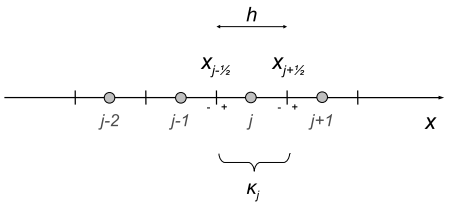


Fig. 1. Mesh with definition of left and right traces at interfaces $x_{j\pm\frac{1}{2}}$.

knowledge of the underlying path. We thus introduce some assumptions on the form of the entropy conservative fluctuation fluxes and derive conditions on the scheme to keep high-order accuracy and a same semi-discrete scheme for the cell averaged approximate solution as in the original DGSEM. The method is fairly general and we provide examples of entropy conservative fluxes for nonconservative systems in various fields such as spray dynamics, gas dynamics, shallow water flows or two-phase flows. A deeper analysis is given for the discretization of the compressible Euler equations in nonconservative form [14] and for two two-phase flow models in one space-dimension: a 2×2 system with a nonconservative product associated to a linearly-degenerate (LD) characteristic field, and the isentropic Baer–Nunziato model. We provide numerical examples where the original DGSEM fails to capture the entropy weak solution. The use of an entropy stable DGSEM scheme is here necessary to capture the correct solution and improve robustness of the computations. For the Baer–Nunziato model, we further analyze the properties of the discrete scheme and derive conditions on the time step to keep positivity of the partial densities and a maximum principle on the void fractions. These properties hold for the cell averaged numerical solution and motivate the use of a posteriori limiters [61,62] to extend them to nodal values within elements. Again, numerical experiments highlight stability and robustness improvement with the entropy stable scheme.

The paper is organized as follows. Section 2 presents the DGSEM for the space discretization of nonconservative systems (1) and its entropy stable version through the use of entropy conservative and entropy stable numerical fluxes. In section 3, we derive the semi-discrete entropy inequality and give conditions on the numerical fluxes to keep high-order accuracy and the semi-discrete scheme for the cell averaged numerical solution. Four examples of entropy conservative fluxes are given in section 4 for different nonconservative systems and some other examples are given in Appendix A. We further investigate the stability and robustness properties of an entropy stable DGSEM for the isentropic Baer–Nunziato model in section 5. Numerical experiments for the four examples of section 4 are given in section 6. Finally, concluding remarks about this work are given in section 7.

2. DGSEM formulation

The DG method consists in defining a semi-discrete weak formulation of problem (1). The domain is discretized with a grid $\Omega_h = \cup_{j\in\mathbb{Z}}\kappa_j$ with cells $\kappa_j = [x_{j-\frac{1}{2}}, x_{j+\frac{1}{2}}]$, $x_{j+\frac{1}{2}} = jh$ and $h > 0$ the space step (see Fig. 1) that we assume to be uniform without loss of generality.

2.1. Numerical solution

We look for approximate solutions in the function space of discontinuous polynomials $\mathcal{V}_h^p = \{v_h \in L^2(\Omega_h) : \ v_h|_{\kappa_j} \in \mathcal{P}_p(\kappa_j),\ \kappa_j \in \Omega_h\}$, where $\mathcal{P}_p(\kappa_j)$ denotes the space of polynomials of degree at most p in the element κ_j. The approximate solution to (1) is sought under the form

$$\mathbf{u}_h(x,t) = \sum_{l=0}^{p} \varphi_j^l(x)\mathbf{U}_j^l(t), \quad \forall x \in \kappa_j,\ \kappa_j \in \Omega_h,\ t \geq 0, \tag{5}$$

where $\mathbf{U}_j^{0\leq l\leq p}$ are the degrees of freedom (DOFs) in the element κ_j. The subset $(\varphi_j^0, \dots, \varphi_j^p)$ constitutes a basis of $\mathcal{V}_h^p$ restricted onto a given element. In this work we will use the Lagrange interpolation polynomials $\ell_{0\leq k\leq p}$ associated to the Gauss–Lobatto nodes over the segment $[-1, 1]$: $s_0 = -1 < s_1 < \cdots < s_p = 1$:

$$\ell_k(s_l) = \delta_{k,l}, \quad 0 \leq k, l \leq p, \tag{6}$$

with $\delta_{k,l}$ the Kronecker symbol. The basis functions with support in a given element κ_j thus write $\varphi_j^k(x) = \ell_k(\sigma_j(x))$ where $\sigma_j(x) = 2(x - x_j)/h$ and $x_j = (x_{j+\frac{1}{2}} + x_{j-\frac{1}{2}})/2$ denotes the center of the element.

The DOFs thus correspond to the point values of the solution: given $0 \leq k \leq p$, j in $\mathbb{Z}$, and $t \geq 0$, we have $\mathbf{u}_h(x_j^k, t) = \mathbf{U}_j^k(t)$ for $x_j^k = x_j + s_k h/2$. The left and right traces of the numerical solution at interfaces $x_{j\pm\frac{1}{2}}$ of a given element hence read (see Fig. 1):

$$\mathbf{u}^-_{j+\frac{1}{2}}(t) := \mathbf{u}_h(x^-_{j+\frac{1}{2}}, t) = \mathbf{U}^p_j(t), \quad \forall t \geq 0, \tag{7a}$$

$$\mathbf{u}^+_{j-\frac{1}{2}}(t) := \mathbf{u}_h(x^+_{j-\frac{1}{2}}, t) = \mathbf{U}^0_j(t), \quad \forall t \geq 0. \tag{7b}$$

It is convenient to introduce the discrete derivative matrix with entries

$$D_{kl} = \ell_l'(s_k) = \frac{h}{2} d_x \varphi^l_j(x^k_j), \quad 0 \leq k, l \leq p. \tag{8}$$

In the DGSEM, the integrals over elements are approximated by using a Gauss–Lobatto quadrature rule with nodes collocated with the interpolation points of the numerical solution

$$\int_{\kappa_j} f(x)dx \simeq \frac{h}{2} \sum_{l=0}^{p} \omega_l f(x^l_j), \tag{9}$$

with $\omega_l > 0$, $x^l_j = x_j + s_l h/2$ the weights and nodes of the quadrature rule which impose $\sum_{l=0}^{p} \omega_l = \int_{-1}^{1} ds = 2$, and s_l the node positions in $[-1, 1]$. This leads to the definition of the discrete inner product in the element κ_j

$$\langle f, g \rangle^p_j := \frac{h}{2} \sum_{l=0}^{p} \omega_l f(x^l_j) g(x^l_j).$$

As noticed in [32], the DGSEM satisfies the summation-by-parts property:

$$\omega_k D_{kl} + \omega_l D_{lk} = \delta_{kl}(\delta_{kp} - \delta_{k0}), \quad 0 \leq k, l \leq p. \tag{10}$$

Note also that the property $\sum_{l=0}^{p} \ell_l \equiv 1$ implies

$$\sum_{l=0}^{p} D_{kl} = 0, \quad 0 \leq k \leq p. \tag{11}$$

2.2. Space discretization

The semi-discrete form of the DG discretization in space of problem (1) reads [29,48]: find $\mathbf{u}_h$ in $(\mathcal{V}^p_h)^m$ such that

$$\begin{aligned} \int_{\Omega_h} v_h \partial_t \mathbf{u_h} dx + \sum_{\kappa_j \in \Omega_h} \int_{\kappa_j} v_h \mathbf{A}(\mathbf{u}_h) \partial_x \mathbf{u}_h dx + \sum_{j \in \mathbb{Z}} v^-_{j+\frac{1}{2}} \mathbf{D}^-\big(\mathbf{u}^-_{j+\frac{1}{2}}(t), \mathbf{u}^+_{j+\frac{1}{2}}(t)\big) \\ + \sum_{j \in \mathbb{Z}} v^+_{j-\frac{1}{2}} \mathbf{D}^+\big(\mathbf{u}^-_{j-\frac{1}{2}}(t), \mathbf{u}^+_{j-\frac{1}{2}}(t)\big) = 0, \quad \forall v_h \in \mathcal{V}^p_h, t > 0, \end{aligned} \tag{12}$$

where the numerical fluxes $\mathbf{D}^{\pm}(\cdot, \cdot)$ in fluctuation form will be defined below.

The projection of the initial condition (1b) onto $(\mathcal{V}^p_h)^m$ reads

$$\int_{\Omega_h} v_h(x) \mathbf{u_h}(x, 0) dx = \int_{\Omega_h} v_h(x) \mathbf{u}_0(x) dx, \quad \forall v_h \in \mathcal{V}^p_h.$$

Substituting v_h for the Lagrange interpolation polynomials (6) and using the Gauss–Lobatto quadrature (9) to approximate the volume integrals, (12) becomes

$$\frac{\omega_k h}{2} \frac{d\mathbf{U}^k_j}{dt} + \omega_k \mathbf{A}(\mathbf{U}^k_j) \sum_{l=0}^{p} \mathbf{U}^l_j D_{kl} + \delta_{kp} \mathbf{D}^-(\mathbf{U}^p_j, \mathbf{U}^0_{j+1}) + \delta_{k0} \mathbf{D}^+(\mathbf{U}^p_{j-1}, \mathbf{U}^0_j) = 0, \quad \forall j \in \mathbb{Z}, \quad 0 \leq k \leq p, \quad t > 0. \tag{13}$$

In section 2.3, we propose to modify the volume integrals in (13) so as to satisfy an entropy balance. Note that (13) satisfies some conservation property:

$$h \frac{d\langle \mathbf{u} \rangle_j}{dt} + \langle \mathbf{A}(\mathbf{u}_h), d_x \mathbf{u}_h \rangle^p_j + \mathbf{D}^-(\mathbf{U}^p_j, \mathbf{U}^0_{j+1}) + \mathbf{D}^+(\mathbf{U}^p_{j-1}, \mathbf{U}^0_j) = 0, \tag{14}$$

for the cell averaged solution

$$\langle \mathbf{u} \rangle_j(t) := \frac{1}{h} \int_{\kappa_j} \mathbf{u}_h(x, t) dx = \frac{1}{2} \sum_{k=0}^{p} \omega_k \mathbf{U}^k_j(t).$$

The numerical fluxes in fluctuation form satisfy the following consistency property

$$\mathbf{D}^{\pm}(\mathbf{u},\mathbf{u}) = 0, \quad \forall \mathbf{u} \in \Omega^a, \tag{15}$$

and may also satisfy the path-conservative property [43]

$$\mathbf{D}^{-}(\mathbf{u}^-,\mathbf{u}^+) + \mathbf{D}^{+}(\mathbf{u}^-,\mathbf{u}^+) = \int_0^1 \mathbf{A}\big(\boldsymbol{\phi}(s;\mathbf{u}^-,\mathbf{u}^+)\big)\partial_s\boldsymbol{\phi}(s;\mathbf{u}^-,\mathbf{u}^+)ds, \tag{16}$$

for a given path $\boldsymbol{\phi}$.

2.3. Entropy stable numerical fluxes

In the following, we use the usual terminology from [12] and denote by *entropy conservative* for the entropy–entropy flux pair (η, q) in (3), the numerical fluxes $\mathbf{D}^{\pm}_{ec}$ satisfying:

$$\boldsymbol{\eta}'(\mathbf{u}^-)^\top \mathbf{D}^{-}_{ec}(\mathbf{u}^-,\mathbf{u}^+) + \boldsymbol{\eta}'(\mathbf{u}^+)^\top \mathbf{D}^{+}_{ec}(\mathbf{u}^-,\mathbf{u}^+) = q(\mathbf{u}^+) - q(\mathbf{u}^-), \quad \forall \mathbf{u}^{\pm} \in \Omega^a. \tag{17}$$

Furthermore, we will assume that the numerical fluxes at interfaces in (13) are *entropy stable* in the following sense:

$$\boldsymbol{\eta}'(\mathbf{u}^-)^\top \mathbf{D}^{-}(\mathbf{u}^-,\mathbf{u}^+) + \boldsymbol{\eta}'(\mathbf{u}^+)^\top \mathbf{D}^{+}(\mathbf{u}^-,\mathbf{u}^+) \geq q(\mathbf{u}^+) - q(\mathbf{u}^-), \quad \forall \mathbf{u}^{\pm} \in \Omega^a. \tag{18}$$

As done in [32,16] for hyperbolic conservation laws, we modify the volume integrals in (13) to satisfy the entropy inequality at the semi-discrete level. The semi-discrete scheme now reads

$$\frac{\omega_k h}{2}\frac{d\mathbf{U}_j^k}{dt} + \mathbf{R}_j^k(\mathbf{u}_h) = 0, \quad \forall j \in \mathbb{Z}, \quad 0 \leq k \leq p, \quad t > 0, \tag{19}$$

with

$$\mathbf{R}_j^k(\mathbf{u}_h) = \omega_k \sum_{l=0}^{p} \tilde{\mathbf{D}}(\mathbf{U}_j^k, \mathbf{U}_j^l) D_{kl} + \delta_{kp}\mathbf{D}^{-}(\mathbf{U}_j^p, \mathbf{U}_{j+1}^0) + \delta_{k0}\mathbf{D}^{+}(\mathbf{U}_{j-1}^p, \mathbf{U}_j^0), \tag{20}$$

and

$$\tilde{\mathbf{D}}(\mathbf{u}^-,\mathbf{u}^+) := \mathbf{D}^{-}_{ec}(\mathbf{u}^-,\mathbf{u}^+) - \mathbf{D}^{+}_{ec}(\mathbf{u}^+,\mathbf{u}^-), \quad \forall \mathbf{u}^{\pm} \in \Omega^a, \tag{21}$$

where $\mathbf{D}^{\pm}_{ec}(\cdot,\cdot)$ are some entropy conservative fluctuation fluxes (17). The reason of using $\tilde{\mathbf{D}}(\mathbf{U}_j^k, \mathbf{U}_j^l)$ instead of $\mathbf{A}(\mathbf{U}_j^k)\mathbf{U}_j^l$ in (20) will be made clear below in equation (25) and constitutes the main ingredient for entropy stability.

3. Properties of the semi-discrete scheme

3.1. Entropy stable scheme

Theorem 3.1 proves a semi-discrete entropy inequality for the scheme (19) together with entropy stable fluxes at interfaces, while Theorem 3.2 establishes high-order accuracy and the preservation of equation (14) for the cell averaged solution.

Theorem 3.1 *(entropy stable DGSEM). Let $\tilde{\mathbf{D}}(\cdot,\cdot)$ defined in (21) with $\mathbf{D}^{\pm}_{ec}(\cdot,\cdot)$ consistent (15) and entropy conservative (17) fluctuation fluxes, and let $\mathbf{D}^{\pm}(\cdot,\cdot)$ be consistent (15) and entropy stable (18) fluctuation fluxes. Then, the semi-discrete DGSEM (19) satisfies the following entropy inequality for the pair (η, q) in (3)*

$$h\frac{d\langle\eta\rangle_j}{dt} + Q(\mathbf{U}_j^p, \mathbf{U}_{j+1}^0) - Q(\mathbf{U}_{j-1}^p, \mathbf{U}_j^0) \leq 0, \tag{22}$$

with $\langle\eta\rangle_j = \sum_{k=0}^{p} \frac{\omega_k}{2}\eta(\mathbf{U}_j^k)$ and either

$$Q(\mathbf{U}_j^p, \mathbf{U}_{j+1}^0) = q(\mathbf{U}_j^p) + \boldsymbol{\eta}'(\mathbf{U}_j^p)^\top \mathbf{D}^{-}(\mathbf{U}_j^p, \mathbf{U}_{j+1}^0), \tag{23}$$

or

$$Q(\mathbf{U}_j^p, \mathbf{U}_{j+1}^0) = q(\mathbf{U}_{j+1}^0) - \boldsymbol{\eta}'(\mathbf{U}_{j+1}^0)^\top \mathbf{D}^{+}(\mathbf{U}_j^p, \mathbf{U}_{j+1}^0). \tag{24}$$

Proof. Left multiplying (19) with $\boldsymbol{\eta}'(\mathbf{U}_j^k)$ and adding up over $0 \le k \le p$, we obtain

$$h\frac{d\langle\eta\rangle_j}{dt} + \sum_{k,l}\omega_k \boldsymbol{\eta}'(\mathbf{U}_j^k)^\top \tilde{\mathbf{D}}(\mathbf{U}_j^k, \mathbf{U}_j^l) D_{kl} + \boldsymbol{\eta}'(\mathbf{U}_j^p)^\top \mathbf{D}^-(\mathbf{U}_j^p, \mathbf{U}_{j+1}^0) + \boldsymbol{\eta}'(\mathbf{U}_j^0)^\top \mathbf{D}^+(\mathbf{U}_{j-1}^p, \mathbf{U}_j^0) = 0,$$

where the second term may be transformed into

$$\begin{aligned}
\sum_{k,l}\omega_k \boldsymbol{\eta}'(\mathbf{U}_j^k)^\top \tilde{\mathbf{D}}(\mathbf{U}_j^k, \mathbf{U}_j^l) D_{kl} &\overset{(21)}{=} \sum_{k,l}\omega_k \boldsymbol{\eta}'(\mathbf{U}_j^k)^\top \big(\mathbf{D}_{ec}^-(\mathbf{U}_j^k, \mathbf{U}_j^l) - \mathbf{D}_{ec}^+(\mathbf{U}_j^l, \mathbf{U}_j^k)\big) D_{kl} \\
&\overset{(10)}{=} \sum_{k,l}\omega_k \boldsymbol{\eta}'(\mathbf{U}_j^k)^\top \mathbf{D}_{ec}^-(\mathbf{U}_j^k, \mathbf{U}_j^l) D_{kl} + \omega_l \boldsymbol{\eta}'(\mathbf{U}_j^k)^\top \mathbf{D}_{ec}^+(\mathbf{U}_j^l, \mathbf{U}_j^k) D_{lk} \\
&\quad - \delta_{kl}(\delta_{kp} - \delta_{k0}) \boldsymbol{\eta}'(\mathbf{U}_j^k)^\top \mathbf{D}_{ec}^+(\mathbf{U}_j^l, \mathbf{U}_j^k) \\
&\overset{(15)}{\underset{k\leftrightarrow l}{=}} \sum_{k,l}\omega_k \big(\boldsymbol{\eta}'(\mathbf{U}_j^k)^\top \mathbf{D}_{ec}^-(\mathbf{U}_j^k, \mathbf{U}_j^l) + \boldsymbol{\eta}'(\mathbf{U}_j^l)^\top \mathbf{D}_{ec}^+(\mathbf{U}_j^k, \mathbf{U}_j^l)\big) D_{kl} \\
&\overset{(17)}{=} \sum_{k,l}\omega_k \big(q(\mathbf{U}_j^l) - q(\mathbf{U}_j^k)\big) D_{kl} \\
&\overset{(11)}{=} \sum_{k,l}\omega_k q(\mathbf{U}_j^l) D_{kl} \\
&\underset{(11)}{\overset{(10)}{=}} q(\mathbf{U}_j^p) - q(\mathbf{U}_j^0),
\end{aligned} \tag{25}$$

where $k \leftrightarrow l$ indicates an inversion of indices k and l in some of the terms. We thus obtain

$$h\frac{d\langle\eta\rangle_j}{dt} + q(\mathbf{U}_j^p) - q(\mathbf{U}_j^0) + \boldsymbol{\eta}'(\mathbf{U}_j^p)^\top \mathbf{D}^-(\mathbf{U}_j^p, \mathbf{U}_{j+1}^0) + \boldsymbol{\eta}'(\mathbf{U}_j^0)^\top \mathbf{D}^+(\mathbf{U}_{j-1}^p, \mathbf{U}_j^0) = 0,$$

and using (23) we get

$$h\frac{d\langle\eta\rangle_j}{dt} + Q(\mathbf{U}_j^p, \mathbf{U}_{j+1}^0) - q(\mathbf{U}_j^0) + \boldsymbol{\eta}'(\mathbf{U}_j^0)^\top \mathbf{D}^+(\mathbf{U}_{j-1}^p, \mathbf{U}_j^0) = 0,$$

and adding $Q(\mathbf{U}_{j-1}^p, \mathbf{U}_j^0) - q(\mathbf{U}_{j-1}^p) - \boldsymbol{\eta}'(\mathbf{U}_{j-1}^p)^\top \mathbf{D}^-(\mathbf{U}_{j-1}^p, \mathbf{U}_j^0) = 0$ from (23) to the right-hand-side, we finally deduce

$$\begin{aligned}
h\frac{d\langle\eta\rangle_j}{dt} + Q(\mathbf{U}_j^p, \mathbf{U}_{j+1}^0) - Q(\mathbf{U}_{j-1}^p, \mathbf{U}_j^0) &= q(\mathbf{U}_j^0) - \boldsymbol{\eta}'(\mathbf{U}_j^0)^\top \mathbf{D}^+(\mathbf{U}_{j-1}^p, \mathbf{U}_j^0) \\
&\quad - q(\mathbf{U}_{j-1}^p) - \boldsymbol{\eta}'(\mathbf{U}_{j-1}^p)^\top \mathbf{D}^-(\mathbf{U}_{j-1}^p, \mathbf{U}_j^0) \overset{(18)}{\le} 0.
\end{aligned} \tag{26}$$

A similar result holds with (24). □

Remark 3.1. Entropy fluxes (23) and (24) are different if (18) is satisfied with a strict inequality in contrast to entropy conservative DGSEM, see Corollary 3.1. We stress that both hold for a given choice of numerical fluxes $\mathbf{D}^\pm(\cdot,\cdot)$, but lead to different expressions of the entropy dissipation rate evaluated at the left face of the cell with (23) (see equation (26)) or at the right face of the cell with (24). We do not know a priori if either (23) or (24) leads to a stronger entropy dissipation and this should be application dependent. Equation (26) is also used in section 4.3 for discussing the entropy dissipation rate at the discrete level for the Euler equations (39).

Entropy conservation then results as an immediate consequence.

Corollary 3.1 *(entropy conservative fluxes). Under the assumptions of Theorem 3.1, the semi-discrete DGSEM (19) is entropy conservative iff the numerical fluxes at interfaces are entropy conservative (17). The numerical entropy flux reads*

$$\begin{aligned}
Q(\mathbf{U}_j^p, \mathbf{U}_{j+1}^0) &= q(\mathbf{U}_j^p) + \boldsymbol{\eta}'(\mathbf{U}_j^p)^\top \mathbf{D}_{ec}^-(\mathbf{U}_j^p, \mathbf{U}_{j+1}^0), \\
&= q(\mathbf{U}_{j+1}^0) - \boldsymbol{\eta}'(\mathbf{U}_{j+1}^0)^\top \mathbf{D}_{ec}^+(\mathbf{U}_j^p, \mathbf{U}_{j+1}^0).
\end{aligned}$$

High-order accuracy and the conservation-like property (14) require further assumptions on the form of the entropy conservative fluxes (21) which are summarized in Theorem 3.2. We stress that this form of fluctuation fluxes is fairly general and includes for instance skew-symmetric splittings (see Corollary 3.2).

Theorem 3.2. *Under the assumptions of Theorem 3.1 and further assuming that the entropy conservative fluctuation fluxes (17) have the following form*

$$\mathbf{D}_{ec}^{\pm}(\mathbf{u}^-,\mathbf{u}^+) = \mathcal{A}^{\pm}(\mathbf{u}^-,\mathbf{u}^+)[\![\mathbf{u}]\!], \tag{27a}$$

$$\mathcal{A}(\mathbf{u}^-,\mathbf{u}^+) := \mathcal{A}^-(\mathbf{u}^-,\mathbf{u}^+) + \mathcal{A}^+(\mathbf{u}^-,\mathbf{u}^+), \tag{27b}$$

$$\mathcal{A}(\mathbf{u}^-,\mathbf{u}^+) + \mathcal{A}(\mathbf{u}^+,\mathbf{u}^-) = \mathbf{A}(\mathbf{u}^-) + \mathbf{A}(\mathbf{u}^+), \tag{27c}$$

$$\mathcal{A}(\mathbf{u},\mathbf{u}) = \mathbf{A}(\mathbf{u}), \tag{27d}$$

for all $\mathbf{u}^{\pm}$ *and* $\mathbf{u}$ *in* Ω^a*, where* $[\![\mathbf{u}]\!] = \mathbf{u}^+ - \mathbf{u}^-$*. Then, the semi-discrete DGSEM (19) is a high-order approximation in space of smooth solutions of the nonconservative equation (1a) which satisfies (14).*

Proof. First, to prove accuracy, it is sufficient to prove that the volume integral in (19) is a high-order approximation of $\mathbf{A}(\mathbf{u})\partial_x\mathbf{u}$ at points x_j^k, $0 \le k \le p$, for smooth enough solutions $\mathbf{u}$. Let $\pi_h^p : L^2(\Omega_h) \cap \mathcal{C}(\Omega_h) \ni u \mapsto \pi_h^p(u) \in \mathcal{V}_h^p$ be the Lagrange projection onto $\mathcal{V}_h^p$ associated to nodes (6). Since the Lagrange interpolation error is of order $\mathcal{O}(h^{p+1})$, we have for u and v in $\mathcal{C}^{p+1}(\Omega_h)$:

$$d_x\pi_h^p(uv)(x) = u(x)d_xv(x) + v(x)d_xu(x) + \mathcal{O}(h^p), \quad \forall x \in \Omega_h. \tag{28}$$

Let $t > 0$, introducing the interpolation polynomial $\mathbf{a}_h^k(x) := \sum_{l=0}^p \mathcal{A}^-(\mathbf{U}_j^k,\mathbf{U}_j^l)\varphi_j^l(x)$, we have $\mathbf{a}_h^k(x_j^k) = \mathcal{A}^-(\mathbf{U}_j^k,\mathbf{U}_j^k)$ and $d_x\mathbf{a}_h^k(x_j^k) = \sum_{l=0}^p \mathcal{A}^-(\mathbf{U}_j^k,\mathbf{U}_j^l)d_x\varphi_j^l(x_j^k)$. Using (28) for the product $\mathbf{a}_h^k\mathbf{u}_h$ at point x_j^k, we obtain

$$\frac{2}{h}\sum_{l=0}^p \mathcal{A}^-(\mathbf{U}_j^k,\mathbf{U}_j^l)\mathbf{U}_j^l D_{kl} = \mathcal{A}^-(\mathbf{U}_j^k,\mathbf{U}_j^k)d_x\mathbf{u}_h(x_j^k) + \frac{2}{h}\sum_{l=0}^p \mathcal{A}^-(\mathbf{U}_j^k,\mathbf{U}_j^l)\mathbf{U}_j^k D_{kl} + \mathcal{O}(h^p).$$

Applying the same rule for $\mathbf{a}_h^k(x) := \sum_{l=0}^p \mathcal{A}^+(\mathbf{U}_j^l,\mathbf{U}_j^k)\varphi_j^l(x)$, we finally obtain

$$\frac{2}{h}\sum_{l=0}^p \mathcal{A}^-(\mathbf{U}_j^k,\mathbf{U}_j^l)(\mathbf{U}_j^l - \mathbf{U}_j^k)D_{kl} = \mathcal{A}^-(\mathbf{U}_j^k,\mathbf{U}_j^k)d_x\mathbf{u}_h(x_j^k) + \mathcal{O}(h^p), \tag{29a}$$

$$\frac{2}{h}\sum_{l=0}^p \mathcal{A}^+(\mathbf{U}_j^l,\mathbf{U}_j^k)(\mathbf{U}_j^l - \mathbf{U}_j^k)D_{kl} = \mathcal{A}^+(\mathbf{U}_j^k,\mathbf{U}_j^k)d_x\mathbf{u}_h(x_j^k) + \mathcal{O}(h^p). \tag{29b}$$

We thus have

$$\begin{aligned}
\frac{2}{h}\sum_{l=0}^p \tilde{\mathbf{D}}(\mathbf{U}_j^k,\mathbf{U}_j^l)D_{kl} &\overset{(27a)}{\underset{(21)}{=}} \frac{2}{h}\sum_{l=0}^p \big(\mathcal{A}^-(\mathbf{U}_j^k,\mathbf{U}_j^l) + \mathcal{A}^+(\mathbf{U}_j^l,\mathbf{U}_j^k)\big)(\mathbf{U}_j^l - \mathbf{U}_j^k)D_{kl} \\
&\overset{(29)}{=} \big(\mathcal{A}^-(\mathbf{U}_j^k,\mathbf{U}_j^k) + \mathcal{A}^+(\mathbf{U}_j^k,\mathbf{U}_j^k)\big)d_x\mathbf{u}_h(x_j^k) + \mathcal{O}(h^p) \\
&\overset{(27b)}{=} \mathcal{A}(\mathbf{U}_j^k,\mathbf{U}_j^k)d_x\mathbf{u}_h(x_j^k) + \mathcal{O}(h^p) \\
&\overset{(27d)}{=} \mathbf{A}(\mathbf{U}_j^k)d_x\mathbf{u}_h(x_j^k) + \mathcal{O}(h^p).
\end{aligned}$$

Then, to obtain (14), we add up (19) over $0 \le k \le p$ and obtain

$$h\frac{d\langle\mathbf{u}\rangle_j}{dt} + \sum_{k=0}^p \omega_k \sum_{l=0}^p \tilde{\mathbf{D}}(\mathbf{U}_j^k,\mathbf{U}_j^l)D_{kl} + \mathbf{D}^-(\mathbf{U}_j^p,\mathbf{U}_{j+1}^0) + \mathbf{D}^+(\mathbf{U}_{j-1}^p,\mathbf{U}_j^0) = 0,$$

where the second term may be transformed into

$$\begin{aligned}
\sum_{k,l}\omega_k\tilde{\mathbf{D}}(\mathbf{U}_j^k,\mathbf{U}_j^l)D_{kl} &\overset{(21)}{=} \sum_{k,l}\omega_k\big(\mathbf{D}_{ec}^-(\mathbf{U}_j^k,\mathbf{U}_j^l) - \mathbf{D}_{ec}^+(\mathbf{U}_j^l,\mathbf{U}_j^k)\big)D_{kl} \\
&\overset{(10)}{=} \sum_{k,l}\omega_k\mathbf{D}_{ec}^-(\mathbf{U}_j^k,\mathbf{U}_j^l)D_{kl} + \omega_l\mathbf{D}_{ec}^+(\mathbf{U}_j^l,\mathbf{U}_j^k)D_{lk} - \delta_{kl}(\delta_{kp} - \delta_{k0})\mathbf{D}_{ec}^+(\mathbf{U}_j^l,\mathbf{U}_j^k) \\
&\overset{(15)}{\underset{k\leftrightarrow l}{=}} \sum_{k,l}\omega_k\big(\mathbf{D}_{ec}^-(\mathbf{U}_j^k,\mathbf{U}_j^l) + \mathbf{D}_{ec}^+(\mathbf{U}_j^k,\mathbf{U}_j^l)\big)D_{kl}
\end{aligned}$$

$$
\begin{aligned}
&\overset{(27a,b)}{=} \sum_{k,l} \omega_k \mathcal{A}(\mathbf{U}_j^k, \mathbf{U}_j^l)(\mathbf{U}_j^l - \mathbf{U}_j^k) D_{kl} \\
&\underset{(27d)}{\overset{(10)}{=}} \sum_{k,l} \omega_k \mathcal{A}(\mathbf{U}_j^k, \mathbf{U}_j^l)\mathbf{U}_j^l D_{kl} + \omega_l \mathcal{A}(\mathbf{U}_j^k, \mathbf{U}_j^l)\mathbf{U}_j^k D_{lk} - \mathbf{A}(\mathbf{U}_j^p)\mathbf{U}_j^p + \mathbf{A}(\mathbf{U}_j^0)\mathbf{U}_j^0 \\
&\underset{k\leftrightarrow l}{\overset{(27c)}{=}} \sum_{k,l} \omega_k \big(\mathbf{A}(\mathbf{U}_j^k) + \mathbf{A}(\mathbf{U}_j^l)\big)\mathbf{U}_j^l D_{kl} - \mathbf{A}(\mathbf{U}_j^p)\mathbf{U}_j^p + \mathbf{A}(\mathbf{U}_j^0)\mathbf{U}_j^0 \\
&\overset{(10)}{=} \sum_{k,l} \omega_k \mathbf{A}(\mathbf{U}_j^k)\mathbf{U}_j^l D_{kl}, \\
&= \langle \mathbf{A}(\mathbf{u}_h), d_x \mathbf{u}_h \rangle_j^p,
\end{aligned}
$$

which completes the proof. □

Now, we consider splittings of the nonconservative product for smooth solutions of the form

$$\mathbf{A}\partial_x \mathbf{u} = \alpha \mathbf{A}\partial_x \mathbf{u} + (1-\alpha)\big(\partial_x(\mathbf{A}\mathbf{u}) - (\partial_x \mathbf{A})\mathbf{u}\big), \quad 0 \le \alpha \le 1. \tag{30}$$

Entropy stable schemes based on the above decomposition fall into the assumptions of Theorem 3.2 as stated below.

Corollary 3.2 *(skew-symmetric splitting). Entropy conservative fluxes in (17) for the splitting (30) read*

$$\mathbf{D}_{ec}^{\pm}(\mathbf{u}^-, \mathbf{u}^+) = \mathcal{A}^{\pm}(\mathbf{u}^-, \mathbf{u}^+)[\![\mathbf{u}]\!], \quad \mathcal{A}^{\pm}(\mathbf{u}^-, \mathbf{u}^+) = \frac{1}{2}\big(\alpha \mathbf{A}(\mathbf{u}^{\pm}) + (1-\alpha)\mathbf{A}(\mathbf{u}^{\mp})\big), \tag{31}$$

and constitute particular cases of the high-order entropy conservative fluxes (27) of Theorem 3.2.

Proof. First, using (31) and (21) to evaluate the volume integral in (19), we obtain

$$
\begin{aligned}
\tilde{\mathbf{D}}(\mathbf{u}^-, \mathbf{u}^+) &= \big(\alpha \mathbf{A}(\mathbf{u}^-) + (1-\alpha)\mathbf{A}(\mathbf{u}^+)\big)[\![\mathbf{u}]\!] \\
&= \alpha \mathbf{A}(\mathbf{u}^-)(\mathbf{u}^+ - \mathbf{u}^-) + (1-\alpha)\mathbf{A}(\mathbf{u}^+)(\mathbf{u}^+ - \mathbf{u}^-) \\
&= \alpha \mathbf{A}(\mathbf{u}^-)\mathbf{u}^+ + (1-\alpha)\big(\mathbf{A}(\mathbf{u}^+)\mathbf{u}^+ - \mathbf{A}(\mathbf{u}^+)\mathbf{u}^-\big),
\end{aligned}
$$

since from (11) the term $\mathbf{A}(\mathbf{u}^-)\mathbf{u}^-$ has no contribution to the volume integral in (20), i.e., $\omega_k \sum_{l=0}^{p} \mathbf{A}(\mathbf{U}_j^k)\mathbf{U}_j^k D_{kl} = 0$. The above relation implies that (21) is a volume discretization of the right-hand-side of (30).

Then, from (27b) we have

$$\mathcal{A}(\mathbf{u}^-, \mathbf{u}^+) = \mathcal{A}^-(\mathbf{u}^-, \mathbf{u}^+) + \mathcal{A}^+(\mathbf{u}^-, \mathbf{u}^+) = \tfrac{1}{2}\big(\mathbf{A}(\mathbf{u}^-) + \mathbf{A}(\mathbf{u}^+)\big),$$

which indeed satisfies (27c, d). □

3.2. Entropy conservative fluxes for conservation laws

In the particular case where (1a) reduces to a conservation law, i.e., $\mathbf{A}(\mathbf{u}) = \mathbf{f}'(\mathbf{u})$, it has been shown in [27,16] that it is possible to satisfy the entropy inequality (22) by using the entropy conservative fluxes $\mathbf{h}_{ec}(\mathbf{u}^-, \mathbf{u}^+)$ from Tadmor [55] which satisfy

$$
\begin{aligned}
[\![\boldsymbol{\eta}']\!]^{\top} \mathbf{h}_{ec}(\mathbf{u}^-, \mathbf{u}^+) &= [\![\boldsymbol{\eta}'^{\top}\mathbf{f} - q]\!], \quad \forall \mathbf{u}^{\pm} \in \Omega^a, \\
\mathbf{h}_{ec}(\mathbf{u}, \mathbf{u}) &= \mathbf{f}(\mathbf{u}), \quad \forall \mathbf{u} \in \Omega^a.
\end{aligned}
$$

The link between the fluctuation fluxes $\mathbf{D}_{ec}^{\pm}(\mathbf{u}^-, \mathbf{u}^+)$ and the conservative flux $\mathbf{h}_{ec}(\mathbf{u}^-, \mathbf{u}^+)$ reads

$$\mathbf{h}_{ec}(\mathbf{u}^-, \mathbf{u}^+) = \mathbf{f}(\mathbf{u}^-) + \mathbf{D}_{ec}^{-}(\mathbf{u}^-, \mathbf{u}^+) = \mathbf{f}(\mathbf{u}^+) - \mathbf{D}_{ec}^{+}(\mathbf{u}^-, \mathbf{u}^+),$$

from which we deduce that

$$\mathbf{D}_{ec}^{-}(\mathbf{u}^-, \mathbf{u}^+) - \mathbf{D}_{ec}^{+}(\mathbf{u}^+, \mathbf{u}^-) = \mathbf{h}_{ec}(\mathbf{u}^-, \mathbf{u}^+) + \mathbf{h}_{ec}(\mathbf{u}^+, \mathbf{u}^-) - 2\mathbf{f}(\mathbf{u}^-), \tag{32}$$

and using (11) the volume integral in (19) becomes

$$\omega_k \sum_{l=0}^{p} \tilde{\mathbf{D}}(\mathbf{U}_j^k, \mathbf{U}_j^l) D_{kl} = \omega_k \sum_{l=0}^{p} \big(\mathbf{h}_{ec}(\mathbf{U}_j^k, \mathbf{U}_j^l) + \mathbf{h}_{ec}(\mathbf{U}_j^l, \mathbf{U}_j^k)\big) D_{kl}. \tag{33}$$

In [16], a slightly different choice has been made: $\tilde{\mathbf{D}}(\mathbf{u}^-,\mathbf{u}^+) := 2\mathbf{h}_{ec}(\mathbf{u}^-,\mathbf{u}^+)$, where $\mathbf{h}_{ec}(\cdot,\cdot)$ is assumed to be symmetric. In fact, it may be easily verified that the properties of Theorem 3.3 in [16] also hold with (33) which may be seen as a generalization of the framework of entropy stable DGSEM to nonsymmetric entropy conservative fluxes by using the symmetrizer $(\mathbf{h}_{ec}(\mathbf{u}^-,\mathbf{u}^+)+\mathbf{h}_{ec}(\mathbf{u}^+,\mathbf{u}^-))/2$.

4. Examples

In this section we consider four different nonconservative scalar equations and systems in one space dimension and provide examples of entropy conservative and entropy stable numerical fluxes that fall into the category considered in Theorems 3.1 and 3.2 in section 2.3. These examples will be used in the numerical experiments of section 6 and some other examples are given in Appendix A for gas dynamics, spray dynamics, shallow water flows, etc. In the following, it is convenient to introduce the average operator $\overline{u} := \frac{u^-+u^+}{2}$.

4.1. Burgers' equation

The inviscid Burgers' equation in nonconservative form reads

$$\partial_t u + u\partial_x u = 0, \tag{34}$$

with entropy $\eta(u) = \frac{u^2}{2}$ and entropy flux $q(u) = \frac{u^3}{3}$. Entropy conservative fluctuation fluxes of the form (27) read

$$D_{ec}^-(u^-,u^+) = \frac{2u^-+u^+}{6}[\![u]\!], \quad D_{ec}^+(u^-,u^+) = \frac{u^-+2u^+}{6}[\![u]\!]. \tag{35}$$

Using (32), with $f(u) = \frac{u^2}{2}$, and looking for an equivalent symmetric entropy conservative flux for conservative equations, we obtain

$$h_{ec}(u^-,u^+) = \frac{D_{ec}^-(u^-,u^+) - D_{ec}^+(u^-,u^+) + 2f(u^-)}{2} = \frac{(u^-)^2+u^-u^++(u^+)^2}{6},$$

which corresponds to the entropy conservative skew-symmetric splitting of the Burgers' equation [53,32]. Note that this skew-symmetric splitting already consists in a nonconservative formulation of the space derivative $\partial_x \frac{u^2}{2} = \frac{2}{3}\partial_x \frac{u^2}{2} + \frac{1}{3}u\partial_x u$ [32].

4.2. Nonconservative product associated to a LD field

Let us introduce the following nonlinear hyperbolic system representative of two-phase flow problems [19] where the LD characteristic field plays the role of interface velocity [17]:

$$\partial_t u + g(\mathbf{u})\partial_x u = 0, \tag{36a}$$

$$\partial_t v + \partial_x f(\mathbf{u}) = 0, \tag{36b}$$

with $g(\mathbf{u}) = u + v$ and $f(\mathbf{u}) = \frac{v^2-u^2}{2}$. The eigenvalues are $g(\mathbf{u})$ associated to the LD field and v associated to a genuinely nonlinear field so the system is strictly hyperbolic over the set of states $\Omega^a = \{(u,v)^\top \in \mathbb{R}^2 : u > 0\}$. It satisfies an entropy inequality for the pair $\eta(\mathbf{u}) = \frac{(u+v)^2}{2}$ and $q(\mathbf{u}) = \frac{(u+v)^3}{3}$.

Entropy conservative fluctuation fluxes are

$$\mathbf{D}_{ec}^-(\mathbf{u}^-,\mathbf{u}^+) = \frac{1}{6}\begin{pmatrix} \big(2g(\mathbf{u}^-)+g(\mathbf{u}^+)\big)[\![u]\!] \\ (2v^-+v^+)[\![v]\!] - (2u^-+u^+)[\![u]\!] \end{pmatrix}, \tag{37a}$$

$$\mathbf{D}_{ec}^+(\mathbf{u}^-,\mathbf{u}^+) = \frac{1}{6}\begin{pmatrix} \big(g(\mathbf{u}^-)+2g(\mathbf{u}^+)\big)[\![u]\!] \\ (v^-+2v^+)[\![v]\!] - (u^-+2u^+)[\![u]\!] \end{pmatrix}. \tag{37b}$$

Note that the regularized system

$$\partial_t u + g(\mathbf{u})\partial_x u = \epsilon\partial_{xx}^2 u, \quad \partial_t v + \partial_x f(\mathbf{u}) = \epsilon\partial_{xx}^2 v,$$

with $\epsilon > 0$ gives

$$\partial_t \eta(\mathbf{u}) + \partial_x q(\mathbf{u}) - \epsilon\partial_{xx}^2\eta(\mathbf{u}) = -\epsilon\big((\partial_x u)^2 + (\partial_x v)^2\big) \le 0,$$

so the associated viscous profiles will give the physically admissible solutions in the limit $\epsilon = 0^+$. Using this result for numerical purposes, we design the following entropy stable flux

$$\mathbf{D}^{\pm}(\mathbf{u}^-,\mathbf{u}^+)=\begin{pmatrix}\frac{2g(\mathbf{u}^{\pm})+g(\mathbf{u}^{\mp})}{6}[\![u]\!]\\ \pm\big(f(\mathbf{u}^{\pm})-\hat{h}(\mathbf{u}^-,\mathbf{u}^+)\big)\end{pmatrix}\pm\epsilon_v[\![\mathbf{u}]\!],\quad \hat{h}(\mathbf{u}^-,\mathbf{u}^+)=\tfrac{f(\mathbf{u}^-)+f(\mathbf{u}^+)}{2}-\tfrac{\beta_s}{2}[\![v]\!],\tag{38}$$

with numerical parameters $\epsilon_v\geq 0$ and $\beta_s\geq 0$. Setting $\epsilon_v=0$, it may be checked that the fluctuations fluxes in (38) are entropy conservative providing that $\beta_s=([\![v]\!]-[\![u]\!]^2/[\![v]\!])/6$. In practice, we set $\beta_s=\max\big(|v^{\pm}|,|g(\mathbf{u}^{\pm})|,([\![v]\!]-[\![u]\!]^2/[\![v]\!])/6,0\big)$ and $\epsilon_v>0$ to get an entropy stable flux.

4.3. Euler equations in nonconservative form

The compressible Euler equations may be written in nonconservative form as

$$\partial_t\rho+\partial_x(\rho u)=0,\tag{39a}$$
$$\partial_t(\rho u)+\partial_x(\rho u^2+\mathrm{p})=0,\tag{39b}$$
$$\partial_t(\rho e)+\partial_x(\rho e u)+\mathrm{p}\partial_x u=0,\tag{39c}$$

with ρ the density, u the velocity, e the specific internal energy. The equations are supplemented with an equation of states for ideal gas, $\mathrm{p}=(\gamma-1)\rho e$, with $\gamma=\frac{C_p}{C_v}$ the ratio of specific heats, and admissible solutions satisfy an entropy inequality for the pair $\eta(\mathbf{u})=-\rho\mathrm{s}$, $q(\mathbf{u})=-\rho u\mathrm{s}$, with $\mathrm{s}=C_v\ln(\mathrm{T}\rho^{1-\gamma})$ and T the temperature. System (39) satisfies the additional conservation law for the total specific energy $E=e+\frac{u^2}{2}$:

$$\partial_t(\rho E)+\partial_x(\rho E u+\mathrm{p}u)=0.\tag{40}$$

We now consider a class of fluctuations fluxes of the form

$$\mathbf{D}^-(\mathbf{u}^-,\mathbf{u}^+)=\begin{pmatrix}h_\rho-\rho^-u^-\\ h_{\rho u}+\mathrm{p}^\star-\rho^-{u^-}^2-\mathrm{p}^-\\ h_{\rho e}-\rho^-u^-e^-+\beta^-[\![u]\!]\end{pmatrix},\quad \mathbf{D}^+(\mathbf{u}^-,\mathbf{u}^+)=\begin{pmatrix}-h_\rho+\rho^+u^+\\ -h_{\rho u}-\mathrm{p}^\star+\rho^+{u^+}^2+\mathrm{p}^+\\ -h_{\rho e}+\rho^+u^+e^++\beta^+[\![u]\!]\end{pmatrix},\tag{41}$$

where the unknown functions h_ρ, $h_{\rho u}$, $h_{\rho e}$, $\mathrm{p}^\star$, and $\beta^\pm$ depend on $\mathbf{u}^\pm$. We look for entropy stable fluxes that further conserve the total energy, so we apply condition (17), with $\eta(\mathbf{u})=\rho E$ and $q(\mathbf{u})=(\rho E+\mathrm{p})u$, and condition (18), with $\eta(\mathbf{u})=-\rho s$ and $q(\mathbf{u})=-\rho u\mathrm{s}$, thus getting the two following relations

$$\big(\overline{u}h_\rho-h_{\rho u}-\mathrm{p}^\star+\beta^++\beta^-\big)[\![u]\!]=0,\tag{42a}$$
$$-C_v h_\rho\big([\![\ln\theta]\!]+(\gamma-1)[\![\ln\rho]\!]\big)+(\overline{\mathrm{p}\theta}-\beta^-\theta^--\beta^+\theta^+)[\![u]\!]+\overline{u}[\![\mathrm{p}\theta]\!]+h_{\rho e}[\![\theta]\!]\geq 0,\tag{42b}$$

where $\theta=\mathrm{T}^{-1}$. Looking for fluxes that satisfy the above relations for all jump values, it can be easily checked that the following choice is total energy preserving and entropy stable

$$h_\rho=\overline{u}\hat{\rho}-k_\rho[\![\rho]\!],\quad h_{\rho u}=\overline{u}h_\rho,\quad h_{\rho e}=\frac{C_v}{\hat{\theta}}h_\rho-k_e[\![e]\!],\quad \mathrm{p}^\star=\frac{\overline{\theta\mathrm{p}}}{\overline{\theta}}-k_p[\![u]\!],\quad \beta^\pm=\frac{\mathrm{p}^\star}{2},\tag{43}$$

where $\hat{a}=\frac{[\![a]\!]}{[\![\ln a]\!]}$ denotes the logarithmic mean [37], providing that the parameters k_ρ, k_e, and k_p are all non negative. Moreover, the fluxes are entropy conservative when $k_\rho=k_e=k_p=0$. In the numerical experiments, we will use the following choice of parameters $k_\rho=\epsilon_v\frac{\overline{\rho c}}{2\overline{\rho}}$ and $k_e=k_p=\epsilon_v\frac{\overline{\rho c}}{2}$ with $\epsilon_v\geq 0$ and c the speed of sound leading to the following dissipation rate of entropy

$$\frac{d\langle\eta\rangle_j}{dt}+\frac{1}{h}\Big(Q(\mathbf{U}_j^p,\mathbf{U}_{j+1}^0)-Q(\mathbf{U}_{j-1}^p,\mathbf{U}_j^0)\Big)=-\frac{\epsilon_v\overline{\rho c}_{j-\frac12}}{2h}\left(\frac{C_p-C_v}{\overline{\rho}}[\![\ln\rho]\!][\![\rho]\!]+\overline{\theta}[\![u]\!]^2-C_v[\![\mathrm{T}]\!][\![\theta]\!]\right)_{x_{j-\frac12}},$$

where $Q(\cdot,\cdot)$ is defined from (23), and may be compared to the dissipation rate for the formal equations

$$\partial_t\eta(\mathbf{u})+\partial_x q(\mathbf{u})=-\frac{4\mu}{3}\left(\theta(\partial_x u)^2-\frac{3\gamma C_v}{4Pr}\partial_x\mathrm{T}\partial_x\theta\right),$$

where $\mu>0$ is the dynamic viscosity coefficient and Pr denotes the Prandtl number. Thus, $\epsilon_v\overline{\rho c}h$ plays the role of viscosity and setting $k_\rho=0$ in the numerical fluxes (43), one recovers a dissipation rate which scales with the physical one for an equivalent Prandtl number $3\gamma/4$ close to the physical value $Pr=0.72$. We recall that the jump conditions depend on the underlying choice of path in (2) which should be consistent with the viscous profile leading to the physically relevant solution [12,40]. The design of the dissipation introduced in the numerical scheme is thus of great importance as many schemes fail to capture the relevant solution [4,14].

4.4. Isentropic Baer–Nunziato model

We finally consider the two-pressure two-velocity isentropic model [7,6] with void fractions α_i, densities ρ_i, velocities u_i, and a general equation of states $\mathrm{p}_i = \mathrm{p}_i(\rho_i)$ with $\mathrm{p}_i'(\rho_i) > 0$ and $\mathrm{p}_i''(\rho_i) < 0$ for phases $i = 1, 2$. It is useful to introduce the specific internal energy e_i and enthalpy h_i of both phases defined by $\rho_i^2 e_i'(\rho_i) = \mathrm{p}_i(\rho_i)$ and $\rho_i \mathrm{h}_i(\rho_i) = \rho_i e_i(\rho_i) + \mathrm{p}_i(\rho_i)$. Likewise, we introduce the speeds of sound $c_i^2(\rho_i) = \mathrm{p}_i'(\rho_i)$.

4.4.1. Two-phase flow model

Neglecting source terms modeling relaxation mechanisms, the governing equations have the form (4) with

$$\mathbf{u} = \begin{pmatrix} \alpha_1 \\ \alpha_1\rho_1 \\ \alpha_1\rho_1 u_1 \\ \alpha_2\rho_2 \\ \alpha_2\rho_2 u_2 \end{pmatrix}, \quad \mathbf{f}(\mathbf{u}) = \begin{pmatrix} 0 \\ \alpha_1\rho_1 u_1 \\ \alpha_1(\rho_1 u_1^2 + \mathrm{p}_1) \\ \alpha_2\rho_2 u_2 \\ \alpha_2(\rho_2 u_2^2 + \mathrm{p}_2) \end{pmatrix}, \quad \mathbf{c}(\mathbf{u})\partial_x \mathbf{u} = \begin{pmatrix} u_2 \\ 0 \\ -\mathrm{p}_1 \\ 0 \\ \mathrm{p}_1 \end{pmatrix} \partial_x \alpha_1, \tag{44}$$

where u_2 and p_1 have been chosen as closure laws for the interface velocity and pressure, respectively. Both phases are assumed to satisfy the saturation condition

$$\alpha_1 + \alpha_2 = 1. \tag{45}$$

The set of states is $\Omega^a = \{\mathbf{u} \in \mathbb{R}^5 : \ \rho_i > 0, \alpha_i > 0, i = 1, 2\}$ and the system satisfies an entropy inequality (3) for the pair

$$\eta(\mathbf{u}) = \sum_{i=1}^{2} \alpha_i \rho_i \Big(\frac{u_i^2}{2} + e_i(\rho_i) \Big), \quad q(\mathbf{u}) = \sum_{i=1}^{2} \alpha_i \rho_i \Big(\frac{u_i^2}{2} + \mathrm{h}_i(\rho_i) \Big) u_i. \tag{46}$$

We stress that the Baer–Nunziato system is only weakly hyperbolic and the assumptions in the introduction exclude resonance effects [9], though the numerical experiments in section 6 will consider solutions close to resonance.

Note that given δ in $\mathbb{R}$, the nonnegative functions $\psi_\delta^+(\alpha_2) = \max(\alpha_2 - \delta, 0)$ and $\psi_\delta^-(\alpha_2) = -\min(\alpha_2 - \delta, 0)$ constitute convex entropies for the Baer–Nunziato system and satisfy the following inequalities in the sense of distributions

$$\partial_t \big(\psi_\delta^\pm(\alpha_2)\rho_2 \big) + \partial_x \big(\psi_\delta^\pm(\alpha_2)\rho_2 u_2 \big) \le 0, \tag{47}$$

which are easily obtained by combining the equations for the void fraction α_2 and the partial density $\alpha_2\rho_2$.

Following the lines of Tadmor's proof of a minimum entropy principle for the equations of gas dynamics [54, section 3], together with the work by Serre on invariant domains for conservation laws [50], a maximum principle holds for the void fractions. This is summarized in the following lemma.

Lemma 4.1 *(maximum principle). The following estimates hold for solutions of the isentropic Baer–Nunziato model (4), (44):*

$$\operatorname*{ess\,inf}_{|x| \le X + t u_2^{max}} \alpha_i^0(x) \le \alpha_i(x,t) \le \operatorname*{ess\,sup}_{|x| \le X + t u_2^{max}} \alpha_i^0(x), \quad \text{for almost all } |x| \le X, \ t > 0, \tag{48}$$

for $i = 1, 2$, where $u_2^{max} = \max_{\mathcal{C}} |u_2|$ over $\mathcal{C} = \{(x,\tau) : \ |x| \le X + (t-\tau)u_2^{max}, \ 0 \le \tau \le t\}$ and $\alpha_i^0(\cdot) = \alpha_i(\cdot, 0)$.

Proof. Integrating (47) over $\mathcal{C}$, we get

$$\int_{\partial\mathcal{C}} \psi_\delta^\pm(\alpha_2)\rho_2(n_t + u_2 n_x) ds \le 0,$$

where $(n_t, n_x) = \big(1 + (u_2^{max})^2\big)^{-1/2}(u_2^{max}, 1)$ denotes the unit normal on $\partial\mathcal{C}$ pointing outward $\mathcal{C}$, so $n_t + u_2 n_x = \big(1 + (u_2^{max})^2\big)^{-1/2}(u_2^{max} + u_2) \ge 0$ by definition of u_2^{max}. We thus obtain

$$0 \le \int_{|x| \le X} \psi_\delta^\pm(\alpha_2)\rho_2 dx \le \int_{|x| \le X + t u_2^{max}} \psi_\delta^\pm(\alpha_2^0)\rho_2^0 dx,$$

where the left inequality follows from positivity of the integrand. Note that the integrations in the above inequalities are justified in the case of weak solutions, see [50, Sec. I.4].

Using the above result with the nonnegative functions $\psi_\delta^-(\alpha)$ with $\delta = \operatorname{ess\,inf}_{|x| \le X + t u_2^{max}} \alpha_2^0$, then $\psi_\delta^+(\alpha)$ with $\delta = \operatorname{ess\,sup}_{|x| \le X + t u_2^{max}} \alpha_2^0$, satisfying $\psi_\delta^\pm(\alpha_2^0) = 0$, we get $\psi_\delta^\pm(\alpha_2) \equiv 0$ almost everywhere in $\{(x,t) : \ |x| \le X\}$. We thus obtain (48) for α_2. The same result also holds for α_1 through the saturation condition (45). □

4.4.2. Entropy conservative numerical fluxes

Let us consider the following fluxes

$$\mathbf{D}_{ec}^{-}(\mathbf{u}^{-},\mathbf{u}^{+}) = \mathbf{h}(\mathbf{u}^{-},\mathbf{u}^{+}) - \mathbf{f}(\mathbf{u}^{-}) + \mathbf{d}^{-}(\mathbf{u}^{-},\mathbf{u}^{+}), \tag{49a}$$

$$\mathbf{D}_{ec}^{+}(\mathbf{u}^{-},\mathbf{u}^{+}) = \mathbf{f}(\mathbf{u}^{+}) - \mathbf{h}(\mathbf{u}^{-},\mathbf{u}^{+}) + \mathbf{d}^{+}(\mathbf{u}^{-},\mathbf{u}^{+}), \tag{49b}$$

with

$$\mathbf{h}(\mathbf{u}^{-},\mathbf{u}^{+}) = \begin{pmatrix} 0 \\ \overline{\alpha_1}\,\overline{u_1}\hat{h}_1(\rho_1^{-},\rho_1^{+}) \\ \overline{\alpha_1}\big(\overline{u_1}^2\hat{h}_1(\rho_1^{-},\rho_1^{+}) + \overline{\mathrm{p}_1}\big) \\ \overline{\alpha_2}\,\overline{u_2}\hat{h}_2(\rho_2^{-},\rho_2^{+}) \\ \overline{\alpha_2}\big(\overline{u_2}^2\hat{h}_2(\rho_2^{-},\rho_2^{+}) + \overline{\mathrm{p}_2}\big) \end{pmatrix}, \quad \mathbf{d}^{\pm}(\mathbf{u}^{-},\mathbf{u}^{+}) = \frac{[\![\alpha_1]\!]}{2}\begin{pmatrix} u_2^{\pm} \pm \beta_s \\ \pm\beta_s\hat{h}_1(\rho_1^{-},\rho_1^{+}) \\ -\mathrm{p}_1^{\pm} \pm \beta_s\overline{u_1}\hat{h}_1(\rho_1^{-},\rho_1^{+}) \\ \mp\beta_s\hat{h}_2(\rho_2^{-},\rho_2^{+}) \\ \mathrm{p}_1^{\pm} \mp \beta_s\overline{u_2}\hat{h}_2(\rho_2^{-},\rho_2^{+}) \end{pmatrix}, \tag{50}$$

where $\beta_s > 0$ is a measure of the spectral radius of $\mathbf{A}(\mathbf{u}_h)$ and will be evaluated in Lemma 5.1.

Lemma 4.2. *The fluctuation fluxes (49), together with the following choice for the numerical fluxes for the partial densities in (50):*

$$\hat{h}_i(\rho_i^{-},\rho_i^{+}) = \begin{cases} \frac{[\![\mathrm{p}_i(\rho_i)]\!]}{[\![\mathrm{h}_i(\rho_i)]\!]} & \text{if } \rho_i^{-} \neq \rho_i^{+}, \\ \rho_i & \text{if } \rho_i^{-} = \rho_i^{+} = \rho_i, \end{cases} \qquad i = 1,2, \tag{51}$$

are entropy conservative.

Proof. Inserting (46) into (17) and using the Leibniz identities

$$[\![\tfrac{u_i^2}{2}]\!] = \overline{u_i}[\![u_i]\!], \quad [\![\alpha_i\mathrm{p}_i u_i]\!] = \overline{\alpha_i}(\overline{\mathrm{p}_i}[\![u_i]\!] + \overline{u_i}[\![\mathrm{p}_i]\!]) + \overline{\mathrm{p}_i u_i}[\![\alpha_i]\!], \quad i = 1,2, \tag{52}$$

we obtain

$$\begin{aligned}
(\boldsymbol{\eta}'^{-})^{\top}\mathbf{D}_{ec}^{-} + \; & (\boldsymbol{\eta}'^{+})^{\top}\mathbf{D}_{ec}^{+} - [\![q]\!] \overset{(49)}{=} [\![\boldsymbol{\eta}'^{\top}(\mathbf{f}-\mathbf{h})]\!] + (\boldsymbol{\eta}'^{-})^{\top}\mathbf{d}^{-} + (\boldsymbol{\eta}'^{+})^{\top}\mathbf{d}^{+} - [\![q]\!] \\
& \overset{(52)}{\underset{(50)}{=}} -\overline{\alpha_1}\,\overline{u_1}\hat{h}_1[\![\mathrm{h}_1 - \tfrac{u_1^2}{2}]\!] - \overline{\alpha_1}(\overline{u_1}^2\hat{h}_1 + \overline{\mathrm{p}_1})[\![u_1]\!] + [\![\alpha_1\rho_1 u_1(\mathrm{h}_1 - \tfrac{u_1^2}{2})]\!] + [\![\alpha_1(\rho_1 u_1^2 + \mathrm{p}_1)u_1]\!] \\
& - \; \overline{\alpha_2}\,\overline{u_2}\hat{h}_2[\![\mathrm{h}_2 - \tfrac{u_2^2}{2}]\!] - \overline{\alpha_2}(\overline{u_2}^2\hat{h}_2 + \overline{\mathrm{p}_2})[\![u_2]\!] + [\![\alpha_2\rho_2 u_2(\mathrm{h}_2 - \tfrac{u_2^2}{2})]\!] + [\![\alpha_2(\rho_2 u_2^2 + \mathrm{p}_2)u_2]\!] \\
& - \; [\![\alpha_1\rho_1(\tfrac{u_1^2}{2} + \mathrm{h}_1)u_1 + \alpha_2\rho_2(\tfrac{u_2^2}{2} + \mathrm{h}_2)u_2]\!] \\
& + \; [\![\alpha_1]\!]\Big[\overline{u_2(\mathrm{p}_2 - \mathrm{p}_1)} - \overline{u_1}\,\overline{\mathrm{p}_1} + \overline{u_2}\,\overline{\mathrm{p}_1} + \tfrac{\beta_s}{2}\Big([\![\mathrm{p}_2 - \mathrm{p}_1]\!] + \hat{h}_1\big([\![\mathrm{h}_1 - \tfrac{u_1^2}{2}]\!] + \overline{u_1}[\![u_1]\!]\big) \\
& - \; \hat{h}_2\big([\![\mathrm{h}_2 - \tfrac{u_2^2}{2}]\!] + \overline{u_2}[\![u_2]\!]\big)\Big)\Big] \\
& \overset{(51)}{=} -\overline{\alpha_1}(\overline{u_1}[\![\mathrm{p}_1]\!] + \overline{\mathrm{p}_1}[\![u_1]\!]) + [\![\alpha_1 u_1 \mathrm{p}_1]\!] - \overline{u_1}\,\overline{\mathrm{p}_1}[\![\alpha_1]\!] \\
& - \; \overline{\alpha_2}(\overline{u_2}[\![\mathrm{p}_2]\!] + \overline{\mathrm{p}_2}[\![u_2]\!]) + [\![\alpha_2 u_2 \mathrm{p}_2]\!] - \overline{u_2}\,\overline{\mathrm{p}_2}[\![\alpha_2]\!] \\
& \overset{(52)}{=} 0,
\end{aligned}$$

which completes the proof. □

Some remarks are in order. The numerical conservation flux $\mathbf{h}(\cdot,\cdot)$ in (49) is symmetric, consistent and differentiable, while the fluctuation fluxes have the form (27a) with $\mathcal{A}(\mathbf{u}^{-},\mathbf{u}^{+}) = (\overline{u_2}, 0, -\overline{\mathrm{p}_1}, 0, \overline{\mathrm{p}_1})^{\top}$ and therefore satisfy (27c, d) and are path-conservative (16) for a linear path in u_2 and p_1. Due to the presence of the nonlinear fluxes $\hat{h}_i$, the $\mathbf{d}^{\pm}$ are examples of fluctuation fluxes in non-splitting form. Finally, the DGSEM with the fluxes (49) is by construction conservative for the mixture density and momentum.

5. High-order DGSEM for the isentropic Baer–Nunziato model

5.1. Entropy stable fluxes

We now focus on the design of a positive and entropy stable DG scheme for the two-pressure two-velocity isentropic model (4) with (44). For that purpose, we introduce the fully discrete scheme for a one-step first-order explicit time discretization and analyze its properties. High-order time integration will be done by using strong-stability preserving explicit Runge–Kutta methods [51] that keep the properties of the first-order in time scheme.

Let $t^{(n)} = n\Delta t$, with $\Delta t > 0$ the time step, set $\lambda = \frac{\Delta t}{h}$, and use the notations $\mathbf{u}_h^{(n)}(\cdot) = \mathbf{u}_h(\cdot, t^{(n)})$ and $\mathbf{U}_j^{k,n} = \mathbf{U}_j^k(t^{(n)})$. The DGSEM scheme for solving the isentropic Baer–Nunziato equations reads

$$\frac{\omega_k h}{2}\frac{\mathbf{U}_j^{k,n+1} - \mathbf{U}_j^{k,n}}{\Delta t} + \mathbf{R}_j^k(\mathbf{u}_h^{(n)}) = 0, \tag{53}$$

with $\mathbf{R}_j^k(\cdot)$ defined in (20) and where the entropy conservative fluxes (49) are used in the definition of (21). We follow the strategy in [12] to design entropy stable fluxes at interfaces:

$$\mathbf{D}^{\pm}(\mathbf{u}^-, \mathbf{u}^+) = \mathbf{D}_{ec}^{\pm}(\mathbf{u}^-, \mathbf{u}^+) \pm \epsilon_v \mathbf{D}_v(\mathbf{u}^-, \mathbf{u}^+)[\![\boldsymbol{\eta}'(\mathbf{u})]\!], \tag{54}$$

with $\epsilon_v \geq 0$ and the positive diagonal matrix

$$\mathbf{D}_v(\mathbf{u}^-, \mathbf{u}^+) = \max(\overline{c_1}, \overline{c_2})\,\mathrm{diag}\Big(0, \tfrac{\overline{\alpha_1\rho_1}}{\overline{u_1}^2+\overline{c_1}^2}, \overline{\alpha_1\rho_1}, \tfrac{\overline{\alpha_1\rho_1}}{\overline{u_1}^2+\overline{c_1}^2}, \overline{\alpha_2\rho_2}\Big). \tag{55}$$

5.2. Properties of the discrete scheme

We have the following results that guarantee positivity of the solution and the maximum principle (48) for general equation of states for the fully discrete solution of the DGSEM.

Theorem 5.1. *Assume that* $\rho_{i,j\in\mathbb{Z}}^{0\leq k\leq p,n} > 0$ *and* $\alpha_{i,j\in\mathbb{Z}}^{0\leq k\leq p,n} > 0$ *for* $i = 1, 2$, *then under the CFL conditions*

$$\lambda \max_{j\in\mathbb{Z}} \max_{0\leq k\leq p} \frac{1}{\omega_k}\left(\langle u_{2,h}^{(n)}, d_x\varphi_j^k\rangle_j^p + \delta_{k,p}\frac{\beta_s - u_{2,j}^{p,n}}{2} + \delta_{k,0}\frac{\beta_s + u_{2,j}^{0,n}}{2}\right) < \frac{1}{2}, \tag{56a}$$

$$\lambda \max_{j\in\mathbb{Z}} \max_{i=1,2}\left(\frac{(\beta_s+\tilde{u}_{i,j}^n)\hat{h}_i(\mathbf{U}_j^{0,n},\mathbf{U}_j^{p,n}) - \rho_{i,j}^{0,n}\tilde{c}_i(\mathbf{U}_j^{0,n},\mathbf{U}_j^{p,n})}{\rho_{i,j}^{0,n}} + \frac{(\beta_s-\overline{u}_{i,j-\frac12}^n)\hat{h}_i(\mathbf{U}_{j-1}^{p,n},\mathbf{U}_j^{0,n}) + \rho_{i,j}^{0,n}\tilde{c}_i(\mathbf{U}_{j-1}^{p,n},\mathbf{U}_j^{0,n})}{\rho_{i,j}^{0,n}},\right.$$
$$\left.\frac{(\beta_s+\overline{u}_{i,j+\frac12}^n)\hat{h}_i(\mathbf{U}_j^{p,n},\mathbf{U}_{j+1}^{0,n}) - \rho_{i,j}^{p,n}\tilde{c}_i(\mathbf{U}_j^{p,n},\mathbf{U}_{j+1}^{0,n})}{\rho_{i,j}^{p,n}} + \frac{(\beta_s-\tilde{u}_{i,j}^n)\hat{h}_i(\mathbf{U}_j^{0,n},\mathbf{U}_j^{p,n}) + \rho_{i,j}^{p,n}\tilde{c}_i(\mathbf{U}_j^{0,n},\mathbf{U}_j^{p,n})}{\rho_{i,j}^{p,n}}\right) < \frac{2}{p(p+1)}, \tag{56b}$$

we have for the cell averages at time $t^{(n+1)}$

$$\langle\alpha_i\rho_i\rangle_j^{(n+1)} > 0, \quad \langle\alpha_i\rangle_j^{(n+1)} > 0, \quad i = 1, 2, \quad j \in \mathbb{Z}, \tag{57}$$

and

$$\langle\alpha_1\rangle_j^{(n+1)} = \sum_{k=0}^{p}\left(\frac{\omega_k}{2} - \lambda\left(\langle u_{2,h}^{(n)}, d_x\varphi_j^k\rangle_j^p + \delta_{k,p}\frac{\beta_s - u_{2,j}^{p,n}}{2} + \delta_{k,0}\frac{\beta_s + u_{2,j}^{0,n}}{2}\right)\right)\alpha_{1,j}^{k,n} + \lambda\frac{\beta_s - u_{2,j}^{p,n}}{2}\alpha_{1,j+1}^{0,n} + \lambda\frac{\beta_s + u_{2,j}^{0,n}}{2}\alpha_{1,j-1}^{p,n}, \quad j \in \mathbb{Z}, \tag{58}$$

is a convex combination of DOFs at time $t^{(n)}$ *where*

$$\beta_s = \max_{j\in\mathbb{Z}} \max_{i=1,2}\left(-u_{2,j}^{0,n}, u_{2,j}^{p,n}, \frac{\rho_{i,j-1}^{p,n}\tilde{c}_i(\mathbf{U}_{j-1}^{p,n},\mathbf{U}_j^{0,n})}{\hat{h}_i(\mathbf{U}_{j-1}^{p,n},\mathbf{U}_j^{0,n})} - \overline{u}_{i,j-\frac12}^n, \tilde{u}_{i,j}^n - \frac{\rho_{i,j}^{p,n}\tilde{c}_i(\mathbf{U}_j^{0,n},\mathbf{U}_j^{p,n})}{\hat{h}_i(\mathbf{U}_j^{0,n},\mathbf{U}_j^{p,n})}, \frac{\rho_{i,j}^{0,n}\tilde{c}_i(\mathbf{U}_j^{0,n},\mathbf{U}_j^{p,n})}{\hat{h}_i(\mathbf{U}_j^{0,n},\mathbf{U}_j^{p,n})}\right.$$
$$\left. - \tilde{u}_{i,j}^n, \overline{u}_{i,j+\frac12}^n - \frac{\rho_{i,j+1}^{0,n}\tilde{c}_i(\mathbf{U}_j^{p,n},\mathbf{U}_{j+1}^{0,n})}{\hat{h}_i(\mathbf{U}_j^{p,n},\mathbf{U}_{j+1}^{0,n})}\right), \tag{59}$$

$\tilde{u}_{i,j}^n = \frac{u_{i,j}^{0,n}+u_{i,j}^{p,n}}{2}$, $\overline{u}_{i,j+\frac12}^n = \frac{u_{i,j}^{p,n}+u_{i,j+1}^{0,n}}{2}$, *and* $\tilde{c}_i(\mathbf{u}^-, \mathbf{u}^+) = \epsilon_v \max(\overline{c_1}, \overline{c_2})\frac{[\![\mathrm{h}_i - \frac{u_i^2}{2}]\!]}{u_i^2+c_i^2}$.

Proof. We know by Theorem 3.2 that the cell averaged semi-discrete DGSEM (19) holds. Thus, summing the first component in (53) over $0 \le k \le p$ gives

$$\begin{aligned}
\langle \alpha_1 \rangle_j^{(n+1)} &:= \sum_{k=0}^{p} \tfrac{\omega_k}{2} \alpha_{1,j}^{k,n+1} \\
&\underset{(54)}{\overset{(53)}{=}} \langle \alpha_1 \rangle_j^{(n)} - \lambda \langle u_{2,h}^{(n)}, \partial_x \alpha_{1,h}^{(n)} \rangle_j^p - \lambda \Big(\mathbf{d}_1^-(\mathbf{U}_j^{p,n}, \mathbf{U}_{j+1}^{0,n}) + \mathbf{d}_1^+(\mathbf{U}_{j-1}^{p,n}, \mathbf{U}_j^{0,n}) \Big) \\
&\underset{(50)}{\overset{(5)}{=}} \sum_{k=0}^{p} \tfrac{\omega_k}{2} \alpha_{1,j}^{k,n} - \lambda \sum_{k=0}^{p} \langle u_{2,h}^{(n)}, d_x \varphi_j^k \rangle_j^p \alpha_{1,j}^{k,n} - \lambda \left(\tfrac{u_{2,j}^{p,n} - \beta_s}{2} (\alpha_{1,j+1}^{0,n} - \alpha_{1,j}^{p,n}) + \tfrac{u_{2,j}^{0,n} + \beta_s}{2} (\alpha_{1,j}^{0,n} - \alpha_{1,j-1}^{p,n}) \right) \\
&= \sum_{k=1}^{p-1} \left(\tfrac{\omega_k}{2} - \lambda \langle u_{2,h}^{(n)}, d_x \varphi_j^k \rangle_j^p \right) \alpha_{1,j}^{k,n} + \left(\tfrac{\omega_0}{2} - \lambda \langle u_{2,h}^{(n)}, d_x \varphi_j^0 \rangle_j^p - \lambda \tfrac{\beta_s + u_{2,j}^{0,n}}{2} \right) \alpha_{1,j}^{0,n} + \lambda \tfrac{\beta_s + u_{2,j}^{0,n}}{2} \alpha_{1,j-1}^{p,n} \\
&+ \left(\tfrac{\omega_p}{2} - \lambda \langle u_{2,h}^{(n)}, d_x \varphi_j^p \rangle_j^p - \lambda \tfrac{\beta_s - u_{2,j}^{p,n}}{2} \right) \alpha_{1,j}^{p,n} + \lambda \tfrac{\beta_s - u_{2,j}^{p,n}}{2} \alpha_{1,j+1}^{0,n},
\end{aligned}$$

which is indeed a convex combination under the conditions (56a) and $\beta_s \ge \max(-u_{2,j}^{0,n}, u_{2,j}^{p,n})$ satisfied by (59).

The positivity of the cell averaged partial densities relies on the techniques introduced in [44,62] to rewrite a conservative high-order scheme for the mean value as a convex combination of positive first-order schemes. Since the equations for partial densities of phases $i = 1, 2$ are conservative, we get by summing the $2i$-th component in (53) over $0 \le k \le p$:

$$\begin{aligned}
\langle \alpha_i \rho_i \rangle_j^{(n+1)} &= \langle \alpha_i \rho_i \rangle_j^{(n)} - \lambda \Big(H_{2i}(\mathbf{U}_j^{p,n}, \mathbf{U}_{j+1}^{0,n}) - H_{2i}(\mathbf{U}_{j-1}^{p,n}, \mathbf{U}_j^{0,n}) \Big) \\
&= \sum_{k=1}^{p-1} \tfrac{\omega_k}{2} \alpha_{i,j}^{k,n} \rho_{i,j}^{k,n} + \tfrac{\omega_p}{2} \left(\alpha_{i,j}^{p,n} \rho_{i,j}^{p,n} - \tfrac{2\lambda}{\omega_p} \Big(H_{2i}(\mathbf{U}_j^{p,n}, \mathbf{U}_{j+1}^{0,n}) - H_{2i}(\mathbf{U}_j^{0,n}, \mathbf{U}_j^{p,n}) \Big) \right) \\
&+ \tfrac{\omega_0}{2} \left(\alpha_{i,j}^{0,n} \rho_{i,j}^{0,n} - \tfrac{2\lambda}{\omega_0} \Big(H_{2i}(\mathbf{U}_j^{0,n}, \mathbf{U}_j^{p,n}) - H_{2i}(\mathbf{U}_{j-1}^{p,n}, \mathbf{U}_j^{0,n}) \Big) \right)
\end{aligned} \tag{60}$$

which is also a convex combination with coefficients $\frac{\omega_k}{2}$ of DOFs and updates of a three-point scheme with numerical flux $H_{2i}(\mathbf{u}^-, \mathbf{u}^+) = \big(\overline{\alpha_i}\,\overline{u_i} - \frac{\beta_s}{2}[\![\alpha_i]\!]\big)\hat{h}_i - \tilde{c}_i(\mathbf{u}^-, \mathbf{u}^+)\overline{\alpha_1 \rho_1}$ from (54) and (50). It remains to show that this scheme is positive. Consider the scheme

$$\alpha \rho_j^{n+1} = \alpha \rho_j^n - \lambda_{FV} \big(H(\mathbf{U}_j^n, \mathbf{U}_{j+1}^n) - H(\mathbf{U}_{j-1}^n, \mathbf{U}_j^n) \big), \tag{61}$$

where we have removed indices on phases for the sake of clarity. This scheme may be easily recast into the form

$$\alpha \rho_j^{n+1} = \big(1 - \lambda_{FV} (C_{j+\frac{1}{2}}^- + C_{j-\frac{1}{2}}^+) \big) \alpha \rho_j^n + \lambda_{FV} C_{j+\frac{1}{2}}^+ \alpha \rho_{j+1}^n + \lambda_{FV} C_{j-\frac{1}{2}}^- \alpha \rho_{j-1}^n$$

with coefficients $C^\pm = \frac{1}{2\rho^\pm} \big((\beta_s \mp \overline{u}) \hat{h} \pm \rho^\pm \tilde{c} \big)$ for which positivity follows from conditions $C_{j\pm\frac{1}{2}}^\pm \ge 0$ and $\lambda_{FV}(C_{j+\frac{1}{2}}^- + C_{j-\frac{1}{2}}^+) \le 1$. Identifying with (60) with $\lambda = \frac{\omega_0}{2} \lambda_{FV} = \frac{\omega_p}{2} \lambda_{FV}$, $\omega_0 = \omega_p = \frac{2}{p(p+1)}$, we obtain conditions (56b) and (59). □

Remark 5.1. In practice, we replace (56) and (59) by the more affordable conditions

$$\lambda \max_{j \in \mathbb{Z}} \max_{0 \le k \le p} \frac{1}{\omega_k} \left(\langle u_{2,h}^{(n)}, d_x \varphi_j^k \rangle_j^p + \delta_{k,p} \tfrac{\beta_s - u_{2,j}^{p,n}}{2} + \delta_{k,0} \tfrac{\beta_s + u_{2,j}^{0,n}}{2} \right) < \frac{1}{2}, \tag{62}$$

and

$$\beta_s = \max_{j \in \mathbb{Z}} \max_{i=1,2} \Big(|u_{i,j-1}^{p,n}| + c_{i,j-1}^{p,n}, |u_{i,j+1}^{0,n}| + c_{i,j+1}^{0,n} \Big). \tag{63}$$

The rationale for this choice is as follows. First, (58) still is a convex combination under (62) and (63). Then, let go back to the three-point scheme (61) and consider polytropic ideal gas: $\mathrm{p} = (\gamma - 1)\rho e$, $\mathrm{h} = \gamma e$, and $c^2 = (\gamma - 1)\mathrm{h}$ with $\gamma > 1$. The positivity condition reads $\beta_s \ge |\overline{u}| + \frac{\rho^\pm \tilde{c}}{\hat{h}}$ with $\frac{\rho^\pm \tilde{c}}{\hat{h}} = \epsilon_v \rho^\pm \overline{c} \frac{[\![\mathrm{h}]\!]}{[\![\mathrm{p}]\!]} \frac{[\![\mathrm{h} - u^2/2]\!]}{\overline{u^2 + c^2}}$. Observe that

$$\frac{[\![\mathrm{p}]\!]}{\rho^\pm [\![\mathrm{h}]\!]} = \frac{(\gamma - 1)\overline{\rho}}{\gamma \rho^\pm} \left(1 + \frac{\overline{e}[\![\rho]\!]}{\overline{\rho}[\![e]\!]} \right) \ge \frac{\gamma - 1}{2\gamma}, \quad \left| \frac{[\![\mathrm{h} - \frac{u^2}{2}]\!]}{\overline{u^2 + c^2}} \right| \le \left| \frac{[\![\mathrm{h}]\!]}{(\gamma - 1)\overline{\mathrm{h}}} \right| + \left| \frac{[\![u^2]\!]}{2\overline{u^2}} \right| \le \frac{\gamma + 1}{\gamma - 1},$$

from positivity of the thermodynamic variables and the fact that $e'(\rho) > 0$. We thus get $\frac{\rho^{\pm}\tilde{c}}{\hat{h}} \leq \frac{2\gamma(\gamma+1)}{(\gamma-1)^2}\epsilon_v\overline{c}$, so (63) implies (59) for $\epsilon_v \leq \frac{(\gamma-1)^2}{2\gamma(\gamma+1)}$. Though this condition seems restrictive, we used $\epsilon_v \simeq \frac{1}{2p+1}$ during the numerical experiments without violating positivity (57) of Theorem 5.1.

The following result is useful to prevent spurious oscillations in the numerical solution. Indeed, the present schemes satisfies the Abgrall's criterion [1] that states that uniform velocity and pressure must remain uniform at all time.

Theorem 5.2 *(Abgrall's criterion). Assume that the velocity and pressure are uniform and equal at time $t^{(n)}$:*

$$u_{i,j}^{k,n} = u, \quad \mathrm{p}_{i,j}^{k,n} = \mathrm{p}, \quad i = 1, 2, \quad \forall j \in \mathbb{Z}, \quad 0 \leq k \leq p, \tag{64}$$

then they remain uniform and equal at time $t^{(n+1)}$.

Proof. The assumption (64) on pressures require uniform densities $\rho_{i,j}^{k,n} = \rho_i$, $i = 1, 2$, so $[\![\boldsymbol{\eta}'(\mathbf{u})]\!] = 0$. Then, the entropy conservative fluxes (49) and entropy stable fluxes (54) reduce to

$$\mathbf{D}^{\pm}(\mathbf{u}^-, \mathbf{u}^+) = \mathbf{D}_{ec}^{\pm}(\mathbf{u}^-, \mathbf{u}^+) = \frac{[\![\alpha_1]\!]}{2}\begin{pmatrix} u \pm \beta_s \\ \rho_1(u \pm \beta_s) \\ \rho_1 u(u \pm \beta_s) \\ -\rho_2(u \pm \beta_s) \\ -\rho_2 u(u \pm \beta_s) \end{pmatrix},$$

so the explicit residuals in (53) become $\mathbf{R}_j^k(\mathbf{u}_h) = R_{1,j}^k(1, \rho_1, \rho_1 u, -\rho_2, -\rho_2 u)^\top$ with

$$R_{1,j}^k = \omega_k u \sum_{l=0}^{p} \alpha_{1,j}^k D_{kl} + \tfrac{\delta_{kp}(u-\beta_s)}{2}[\![\alpha_1]\!]_{j+\frac{1}{2}} + \tfrac{\delta_{k0}(u+\beta_s)}{2}[\![\alpha_1]\!]_{j-\frac{1}{2}}, \tag{65a}$$

$$\underset{(11)}{\overset{(45)}{=}} -\omega_k u \sum_{l=0}^{p} \alpha_{2,j}^k D_{kl} - \tfrac{\delta_{kp}(u-\beta_s)}{2}[\![\alpha_2]\!]_{j+\frac{1}{2}} - \tfrac{\delta_{k0}(u+\beta_s)}{2}[\![\alpha_2]\!]_{j-\frac{1}{2}}. \tag{65b}$$

We thus rewrite (53) as

$$\tfrac{\omega_k h}{2}\tfrac{\alpha_{1,j}^{k,n+1} - \alpha_{1,j}^{k,n}}{\Delta t} + R_{1,j}^{k,n} = 0, \tag{66a}$$

$$\tfrac{\omega_k h}{2}\tfrac{\alpha_{1,j}^{k,n+1}(\rho_{1,j}^{k,n+1} - \rho_1) + \rho_1(\alpha_{1,j}^{k,n+1} - \alpha_{1,j}^{k,n})}{\Delta t} + \rho_1 R_{1,j}^{k,n} = 0, \tag{66b}$$

$$\tfrac{\omega_k h}{2}\tfrac{(\alpha_1\rho_1)_j^{k,n+1}(u_{1,j}^{k,n+1} - u) + u\big((\alpha_1\rho_1)^{k,n+1} - \rho_1\alpha_{1,j}^{k,n}\big)}{\Delta t} + \rho_1 u R_{1,j}^{k,n} = 0, \tag{66c}$$

$$\tfrac{\omega_k h}{2}\tfrac{\alpha_{2,j}^{k,n+1}(\rho_{2,j}^{k,n+1} - \rho_2) + \rho_2(\alpha_{2,j}^{k,n+1} - \alpha_{2,j}^{k,n})}{\Delta t} - \rho_2 R_{1,j}^{k,n} = 0, \tag{66d}$$

$$\tfrac{\omega_k h}{2}\tfrac{(\alpha_2\rho_2)_j^{k,n+1}(u_{2,j}^{k,n+1} - u) + u\big((\alpha_2\rho_2)^{k,n+1} - \rho_2\alpha_{2,j}^{k,n}\big)}{\Delta t} - \rho_2 u R_{1,j}^{k,n} = 0. \tag{66e}$$

Then, (66b)$-\rho_1\times$(66a) implies $\rho_{1,j}^{k,n+1} = \rho_1$, while (66c)$-\rho_1 u\times$(66a) gives $u_{1,j}^{k,n+1} = u$. Then, using (65) and (66d, e) we obtain $\rho_{2,j}^{k,n+1} = \rho_2$ and $u_{2,j}^{k,n+1} = u$. □

5.3. Limiting strategy

The properties in Theorem 5.1 hold only for the cell averaged value of the numerical solution at time $t^{(n+1)}$, which is not sufficient for robustness and stability of numerical computations. However, these results motivate the use of a posteriori limiters introduced in [61,62]. These limiters aim at extending preservation of invariant domains [62] or maximum principle [61] from mean values to nodal values within elements.

We enforce positivity of nodal values of partial densities and the maximum principle (48) by using the linear limiter

$$\tilde{\mathbf{U}}_j^{k,n+1} = \theta_j(\mathbf{U}_j^{k,n+1} - \langle\mathbf{u}\rangle_j^{(n+1)}) + \langle\mathbf{u}\rangle_j^{(n+1)}, \quad 0 \leq k \leq p, \quad j \in \mathbb{Z}, \tag{67}$$

with $0 \leq \theta_j \leq 1$ defined by $\theta_j := \min(\theta_j^{\rho_i}, \theta_j^{\alpha_i} : i = 1, 2)$ where

$$\theta_j^{\rho_i} = \min\Big(\frac{\langle\rho_i\rangle_j^{(n+1)} - \epsilon}{\langle\rho_i\rangle_j^{(n+1)} - \rho_{i,j}^{min}}, 1\Big), \quad \rho_{i,j}^{min} = \min_{0\le k\le p} \rho_{i,j}^{k,n+1},$$

$$\theta_j^{\alpha_i} = \min\Big(\frac{\langle\alpha_i\rangle_j^{(n+1)} - m_j^{\alpha_i}}{\langle\alpha_i\rangle_j^{(n+1)} - \alpha_{i,j}^{min}}, \frac{\langle\alpha_i\rangle_j^{(n+1)} - M_j^{\alpha_i}}{\langle\alpha_i\rangle_j^{(n+1)} - \alpha_{i,j}^{max}}, 1\Big), \quad \alpha_{i,j}^{min} = \min_{0\le k\le p} \alpha_{i,j}^{k,n+1}, \quad \alpha_{i,j}^{max} = \max_{0\le k\le p} \alpha_{i,j}^{k,n+1},$$

$0 < \epsilon \ll 1$ is a parameter (we set $\epsilon = 10^{-8}$ in our numerical tests), and

$$m_j^{\alpha_i} = \min\big(\alpha_{i,j-1}^{p,n}, \alpha_{i,j}^{0\le k\le p,n}, \alpha_{i,j+1}^{0,n}\big), \quad M_j^{\alpha_i} = \max\big(\alpha_{i,j-1}^{p,n}, \alpha_{i,j}^{0\le k\le p,n}, \alpha_{i,j+1}^{0,n}\big).$$

The limiter (67) guarantees that $\tilde\rho_j^{0\le k\le p,n+1} \ge \epsilon$ together with a discrete maximum principle on the void fractions $m_j^{\alpha_i} \le \tilde\alpha_{i,j}^{0\le k\le p,n+1} \le M_j^{\alpha_i}$. It also keeps the entropy inequality (3) at the discrete level in the sense that [16, Lemma 3.1] for η convex we have

$$\langle\tilde\eta\rangle_j^{(n+1)} := \sum_{k=0}^{p} \frac{\omega_k}{2} \eta(\tilde{\mathbf{U}}_j^{k,n+1}) \le \langle\eta\rangle_j^{(n+1)}.$$

Likewise, phase densities and velocities remain unchanged by the limiter (67) so uniform velocity and pressure profiles are conserved.

6. Numerical experiments

In the following, we consider Riemann problems for the nonconservative systems introduced in section 4 associated to initial conditions

$$\mathbf{u}_0(x) = \begin{cases} \mathbf{u}_L, & x < 0, \\ \mathbf{u}_R, & x > 0. \end{cases}$$

The set of initial conditions $\mathbf{u}_0$ is given in Table 1. For the time integration, we use the 3-stage third-order strong-stability preserving Runge–Kutta time integration scheme of Shu and Osher [51].

6.1. Entropy conservative schemes

We first validate the entropy conservation property of the modified numerical scheme (19)–(21) stated in Corollary 3.1 which constitutes the basis of the theoretical results of section 3. We follow the experimental setup introduced in [10]. We consider some examples of section 4 and use the corresponding entropy conservative fluxes in (20) and (21) and choose an initial condition resulting in the development of an isolated shock wave with a moderate strength (see Table 1) on a domain of unit length with periodic boundary conditions. As a result of entropy conservation of the space discretization, only the time integration scheme should modify the global entropy budget at the discrete level. We thus evaluate the difference

$$\mathcal{E}_\Omega(t) := \Big|\sum_j \langle\eta(\mathbf{u}_h)\rangle_j(t) - \langle\eta(\mathbf{u}_0)\rangle_j\Big|, \tag{68}$$

which quantifies the difference between the discrete entropy at final time and the initial entropy over the domain Ω_h.

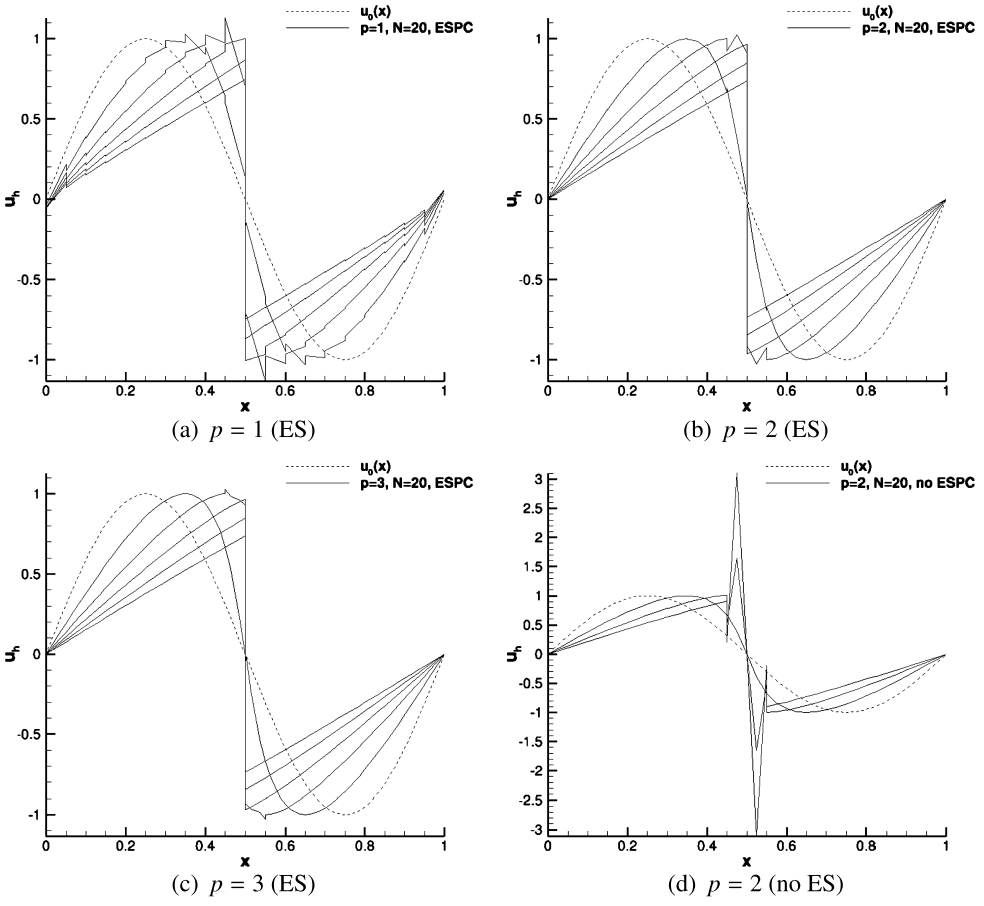
Results are shown in Table 2, for Examples 4.1 to 4.4. We use a space grid of $N = 100$ elements and fourth-order accuracy in space $p = 3$. For the Euler equations, we use the initial condition from [10] and test the entropy conservation with numerical fluxes (41) with numerical parameter $\epsilon_v = 0$ for $\eta(\mathbf{u}) = -\rho s$, and $\epsilon_v = 1$ for $\eta(\mathbf{u}) = \rho E$. We observe that the errors (68) decrease to machine accuracy when refining the time step with an experimental order of convergence of order three corresponding to the theoretical approximation order of the time integration scheme, thus validating the entropy conservative property of the numerical schemes.

6.2. Riemann problems

We now consider more challenging test cases and test the effect of the present method on the robustness and stability of numerical computations of discontinuous solutions. Figs. 3 to 7 compare the numerical solution in symbols with the exact solution in lines.

We evaluate the time step with a safety factor of $\Delta t = 0.9 \times \lambda h$, where λ is evaluated from

$$\lambda \max_{j\in\mathbb{Z}} \Big(\max_{0\le k\le p} \rho_s(\mathbf{A}(\mathbf{U}_k^{k,n})), \frac{2\epsilon_v h}{2p+1} \Big) \le \frac{1}{2p+1},$$



(a) $p = 1$ (ES) (b) $p = 2$ (ES)

(c) $p = 3$ (ES) (d) $p = 2$ (no ES)

Fig. 2. Burgers: solution obtained at different times $t = 0.1$, 0.2, 0.3, 0.4, and 0.5 for a polynomial degree p, $N = 20$ cells and entropy stable (ES) modification (21) or not (no ES).

where $\rho_s(\cdot)$ denotes the spectral radius, for Examples 4.1 to 4.3 and from (62) for the isentropic Baer–Nunziato model.

Entropy stable schemes at element interfaces are obtained by adding viscosity operators that mimic, at the discrete level, a physical parabolic regularization in the same way as done in [12]. These operators are introduced in sections 4.2, 4.3 and 5. Let us stress that we here consider systems (36) and (4), (44) having nonconservative products associated with LD characteristic fields for which finite difference schemes have been shown to converge to the physically relevant solution [13]. However the present strategy may fail for strong shocks where the agreement between regularizations at discrete and continuous levels may not be satisfied [13].

6.2.1. Burgers' equation

We use the entropy conservative fluxes (35) in the volume integral (21), while we use the following fluctuation fluxes at interfaces

$$D^{\pm}(u^-,u^+) = \mp h(u^-,u^+) \pm u^{\pm}, \quad h(u^-,u^+) = \begin{cases} \min\{\frac{v^2}{2} : v \in [u^-,u^+]\}, & \text{if } u^- \le u^+, \\ \max\{\frac{v^2}{2} : v \in [u^+,u^-]\}, & \text{if } u^- > u^+, \end{cases} \tag{69}$$

where $h(\cdot,\cdot)$ is the Godunov numerical flux and is entropy stable.

Fig. 2 displays solutions at different times obtained with the nonconservative Burgers' equation (34) and a smooth initial condition $u_0(x) = \sin(2\pi x)$. Results highlight the good resolution of the shock wave and the decrease of oscillations within cells while p is increased with the entropy stable scheme. In contrast, using the same numerical flux at interfaces (69) with the original form of the volume integral in (13) leads to large oscillations which amplify in time when the solution becomes discontinuous as observed in Fig. 2d.

6.2.2. Nonconservative product associated to a LD field

Fig. 3 shows results for a 1-shock, 2-contact problem (RP0 in Table 1) for system (36). We compare solutions obtained with the entropy stable scheme (19), with (21) evaluated from the entropy conservative fluxes (37), or with the original

Table 1
Initial conditions and physical parameters of Riemann problems with $\boldsymbol{\mathcal{U}} = u$ for the Burgers' equation (34), $\boldsymbol{\mathcal{U}} = (u, v)^\top$ for the 2×2 system (36), $\boldsymbol{\mathcal{U}} = (\rho, u, \mathrm{p})^\top$ for the Euler system (39), and $\boldsymbol{\mathcal{U}} = (\alpha_1, \rho_1, u_1, \rho_2, u_2)^\top$ for the isentropic Baer–Nunziato system (4), (44).

Test	Model	Left state $\boldsymbol{\mathcal{U}}_L$	Right state $\boldsymbol{\mathcal{U}}_R$	t
EC1	(34)	1.1	1	0.1
EC2	(36)	$(0.5, 1.1)^\top$	$(0.5, 1)^\top$	0.15
RP0	(36)	$(3, 0.5)^\top$	$(0.75, 1)^\top$	0.15
EC3	(39)	$(1, 0, 1)^\top$	$(1.125, 0, 1.1)^\top$	0.5
shock	(39)	$(0.4765625, 2.3046638387921279, 1)^\top$	$(0.125, 0, 0.1)^\top$	0.1
Sod	(39)	$(1, 0, 1)^\top$	$(0.125, 0, 0.1)^\top$	0.2
Lax	(39)	$(0.445, 0.698, 3.528)^\top$	$(0.5, 0, 0.571)^\top$	0.13
EC4	(4), (44)	$\begin{pmatrix} 0.5 \\ 1 \\ 1 \\ 1 \\ 1 \end{pmatrix}$	$\begin{pmatrix} 0.5 \\ 1.1 \\ 0.9318181818181817 \\ 1.1 \\ 0.9318181818181817 \end{pmatrix}$	0.15
RP1	(4), (44)	$\begin{pmatrix} 0.1 \\ 0.85 \\ 0.4609513139 \\ 0.96 \\ 0.0839315299 \end{pmatrix}$	$\begin{pmatrix} 0.6 \\ 1.2520240113 \\ 0.7170741165 \\ 0.2505659851 \\ -0.3764790609 \end{pmatrix}$	0.14
RP2	(4), (44)	$\begin{pmatrix} 0.999 \\ 1.8 \\ 0.747051068928543 \\ 3.979765198025580 \\ 0.6 \end{pmatrix}$	$\begin{pmatrix} 0.4 \\ 2.081142099494683 \\ 0.267119045902047 \\ 5.173694757433254 \\ 1.069067604724276 \end{pmatrix}$	0.1
RP3	(4), (44)	$\begin{pmatrix} 0.29 \\ 2.0059425069187893 \\ 65 \\ 2.0059425069187893 \\ 1 \end{pmatrix}$	$\begin{pmatrix} 0.3 \\ 2.0059425069187893 \\ 50 \\ 2.0059425069187893 \\ 1 \end{pmatrix}$	0.08

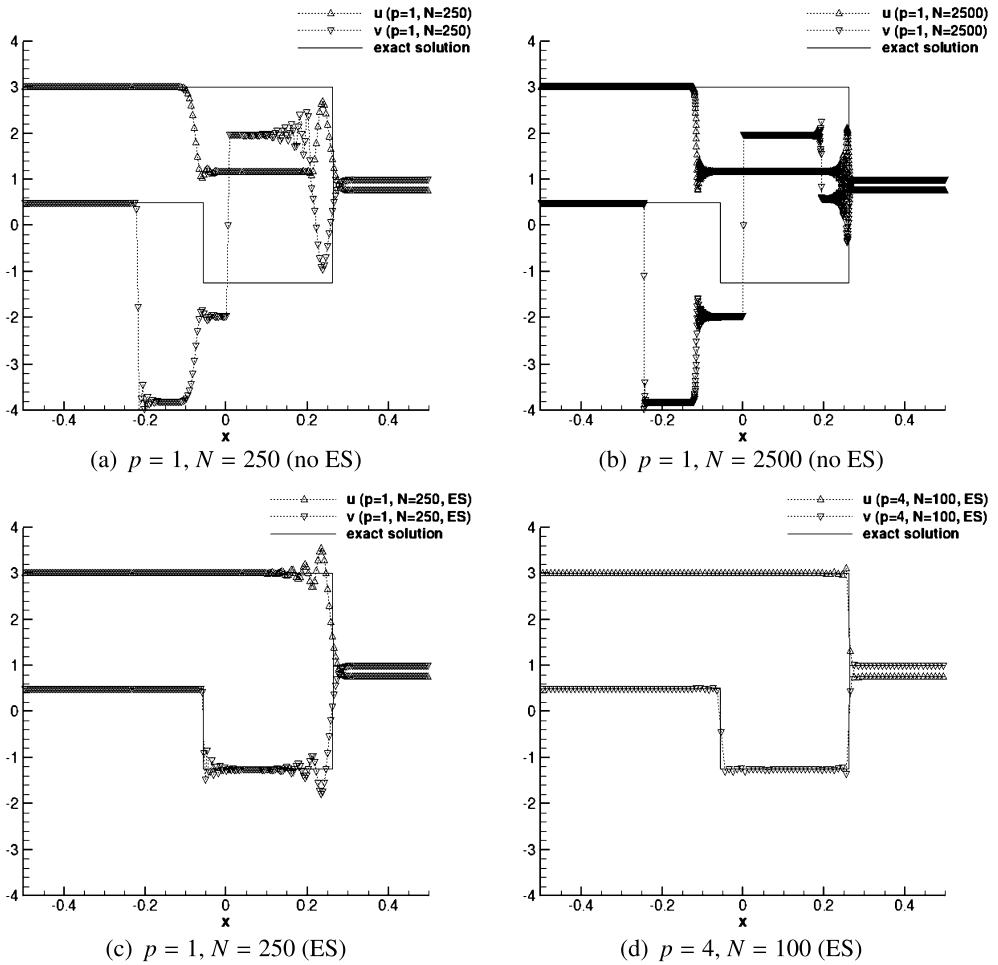
Table 2
Entropy conservation error (68) and corresponding order of convergence $\mathcal{O}$ (see Table 1 for a description of the test cases).

Test case	EC1		EC2		EC3 ($\eta(\mathbf{u}) = -\rho s$)		EC3 ($\eta(\mathbf{u}) = \rho E$)		EC4	
	$\mathcal{E}_\Omega(t)$	$\mathcal{O}$	$\mathcal{E}_\Omega(t)$	$\mathcal{O}$	$\mathcal{E}_\Omega(t)$	$\mathcal{O}$	$\mathcal{E}_\Omega(t)$	$\mathcal{O}$	$\mathcal{E}_\Omega(t)$	$\mathcal{O}$
Δt	6.6310e−06	–	5.3463e−07	–	9.5312e−07	–	2.3712e−06	–	1.2134e−07	–
$\Delta t/2$	1.9086e−06	1.80	7.0781e−08	2.92	2.4818e−07	1.94	6.1800e−07	1.94	1.5786e−08	2.94
$\Delta t/4$	2.8396e−07	2.75	8.9489e−09	2.98	3.5602e−08	2.80	8.8700e−08	2.80	2.0335e−09	2.96
$\Delta t/8$	3.6485e−08	2.96	1.1206e−09	3.00	4.5374e−09	2.97	1.1303e−08	2.97	2.5627e−10	2.99
$\Delta t/16$	4.5811e−09	3.00	1.4004e−10	3.00	5.6837e−10	3.00	1.4137e−09	3.00	3.1668e−11	3.02
$\Delta t/32$	5.7291e−10	3.00	1.7320e−11	3.02	7.0299e−11	3.02	1.7074e−10	3.05	3.1352e−12	3.34
$\Delta t/64$	7.1240e−11	3.01	1.7950e−12	3.27	7.2221e−12	3.28	9.2604e−12	4.20	1.2636e−12	1.31

DGSEM (13). In both cases, we use the same entropy stable numerical fluxes (38) at interfaces. The results highlight the importance of the modification of the volume integral in (19) to satisfy the entropy inequality. The second order solution without this modification does not tend to the exact weak solution and contains non-physical waves even when the mesh is refined. We note that higher-order computations for $p \geq 2$ without the correction (21) were seen to blow up due to a change of sign in the u component of the solution which induces a loss of strict hyperbolicity of system (36). The correction (21) successfully stabilizes the computations and the numerical solution now tends to the exact entropy solution.

6.2.3. Nonconservative Euler equations

Again, we first analyze the effect of the formulation of the volume integral. The results are shown in Fig. 4 for a third-order discretization of an isolated shock wave [14] (test "shock" in Table 1) where we compare two different schemes with entropy stable fluxes (41) at interfaces: (ES) with the modified volume integral (19) built with entropy conservative fluxes from (41); (no ES) with the original volume integral (13). As a consequence, the latter scheme is not entropy stable. The entropy stable DGSEM scheme is seen to converge to the physically relevant shock solution, while a spurious discontinuity is observed with the original volume integral for which more artificial viscosity in the numerical fluxes, $\epsilon_v = 2$ in the



(a) $p = 1$, $N = 250$ (no ES) (b) $p = 1$, $N = 2500$ (no ES)

(c) $p = 1$, $N = 250$ (ES) (d) $p = 4$, $N = 100$ (ES)

Fig. 3. 2×2 system: RP0 discretized with polynomial degree p, N cells and entropy stable (ES) modification (21) or not (no ES).

parameters of (43), was necessary to stabilize the computation. The rather simplicity of the numerical fluxes (41) may be compared to the inability of the path-conservative Roe-type fluxes [43] to capture the entropy solution as pointed out in [4,14] and to the relative complexity of the correction proposed by [14] relying on Glimm's random sampling strategy in the context of first-order finite volume methods.

Fig. 5 displays the solutions obtained for the three Riemann problems of Table 1 with a fourth-order entropy stable scheme with fluxes (41) and an artificial viscosity parameter $\epsilon_v = 1$. We observe a sharp capture of shock and contact waves as well as a very good resolution of the rarefaction waves. However, high-frequency oscillations develop in the neighborhood of contacts and cover a large region for the Lax problem. These oscillations are not damped by the scheme even with a large dissipation coefficient ϵ_v and their amplitude increases with p (results not shown here). They may be related to the fact that the dissipation is introduced in the numerical scheme only through interfaces, so internal DOFs $\mathbf{U}_k^{0<k<p}$ may suffer from a lack of stabilization mechanisms. As a consequence, entropy stability holds for the cell-averaged scheme and only large scale components of the error are damped efficiently.

6.2.4. Isentropic Baer–Nunziato model

For the numerical experiments on the isentropic Baer–Nunziato model (4), (44), we consider polytropic ideal gas with equations of state of the form $\mathrm{p}_i(\rho_i) = \kappa \rho_i^{\gamma_i}$ with $\kappa > 0$ and $\gamma_i > 1$, $i = 1, 2$. Computations are done with the entropy stable numerical scheme (53) and fourth-order accuracy, $p = 3$. The limiter (67) is applied at the end of each stage unless stated otherwise. Problems RP1 and RP2 come from [18], while RP3 is adapted from [42].

We first consider the advection of a discontinuity in the void fraction with uniform velocities, $u_{1,0} = u_{2,0} = 1$ and pressures, $\mathrm{p}_{1,0} = \mathrm{p}_{2,0} = 1.25$, so the mass and momentum equations in (4), (44) are trivially satisfied. The pressure law parameters are $\kappa = 1$, $\gamma_1 = 1.4$, and $\gamma_2 = 1.2$. Fig. 6 presents the solution obtained at time $t = 0.1$ with and without limiter. In both cases, the velocities and pressures remain uniform as expected from Theorem 5.2, but the limiter is seen to introduce numerical dissipation that smears the contact discontinuity. The design of a sharp limiter would help to improve the solution but is beyond the scope of the present study where we rather focus on stability and robustness issues.

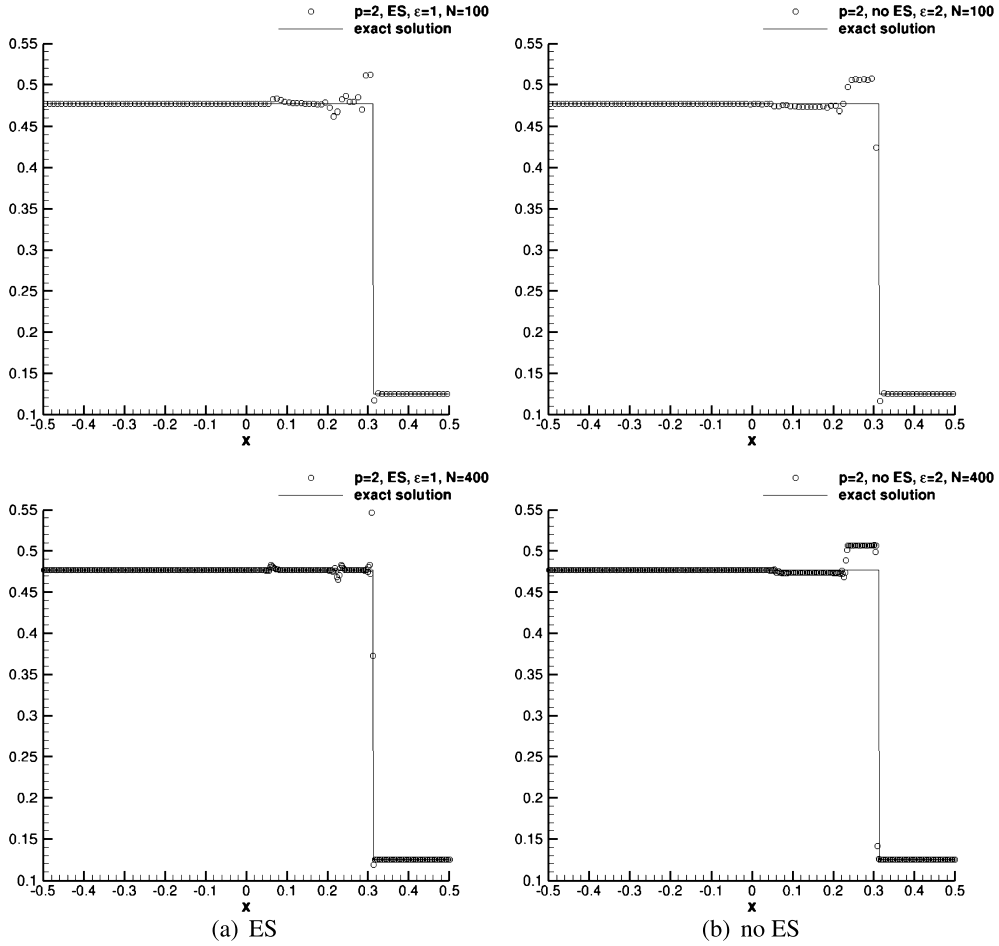


Fig. 4. Euler equations: density profiles for the shock problem discretized with a polynomial degree $p = 2$, $N = 100$ or $N = 400$ cells and entropy stable numerical fluxes (41) at interfaces; (a) scheme (19), (41), (b) scheme (13), (41).

Fig. 7 presents the solution of Riemann problems associated to the initial conditions of Table 1. For RP1 and RP2, we use $\kappa = 1$, $\gamma_1 = 3$ and $\gamma_2 = 1.5$. RP2 considers solutions close to resonance with a vanishing phase 2 and the contact discontinuity separates a mixture region where the two phases coexist from a single phase region. The shock and rarefaction waves are well captured, while the contact wave is slightly diffused as an effect of the limiter as observed in the precedent experiment. RP3 is adapted from the experiment with large relative velocity for one pressure models in [42] and we set $\kappa = 10^5$ and $\gamma_1 = \gamma_2 = 1.4$. Spurious oscillations of low amplitude are observed in the neighborhood of the strong shocks as a result of the limiter (67) which only guarantees positivity by reducing the amplitude of these oscillations, but the results are in good quantitative agreement with the exact solution. We stress that our experiments show that the correction (21) of the volume integral is strongly needed for stabilizing the computations which would blow up otherwise.

7. Concluding remarks

In this work, we introduce a general framework for the design of entropy stable DGSEM for the discretization of nonlinear hyperbolic systems in nonconservative form. The framework relies on the use of SBP operators and two-point entropy conservative fluctuation fluxes [12] to evaluate the integral over discretization elements, thus removing its contribution to the global entropy production within the element, together with entropy stable fluxes at element interfaces. This contribution may be seen as a generalization of the framework on entropy stable spectral collocation schemes for conservation laws introduced in [27,11,32,16]. In particular, the generalizations to multiple space dimensions with quadrangles, hexahedra, or simplex elements; the use of bound-preserving or TVD limiters; and the discretization of viscous terms will keep the entropy inequality for the DGSEM as shown in [16].

Applications show that the method proves to be robust, stable and entropy satisfying for the high-order discretization of the nonconservative Burgers and Euler equations, and two-phase flow models: a 2×2 system with a nonconservative product associated to a LD field and the isentropic Baer–Nunziato model. Numerical experiments show that the proposed modification of the integral over discretization elements has a very beneficial effect on the stability and robustness of the

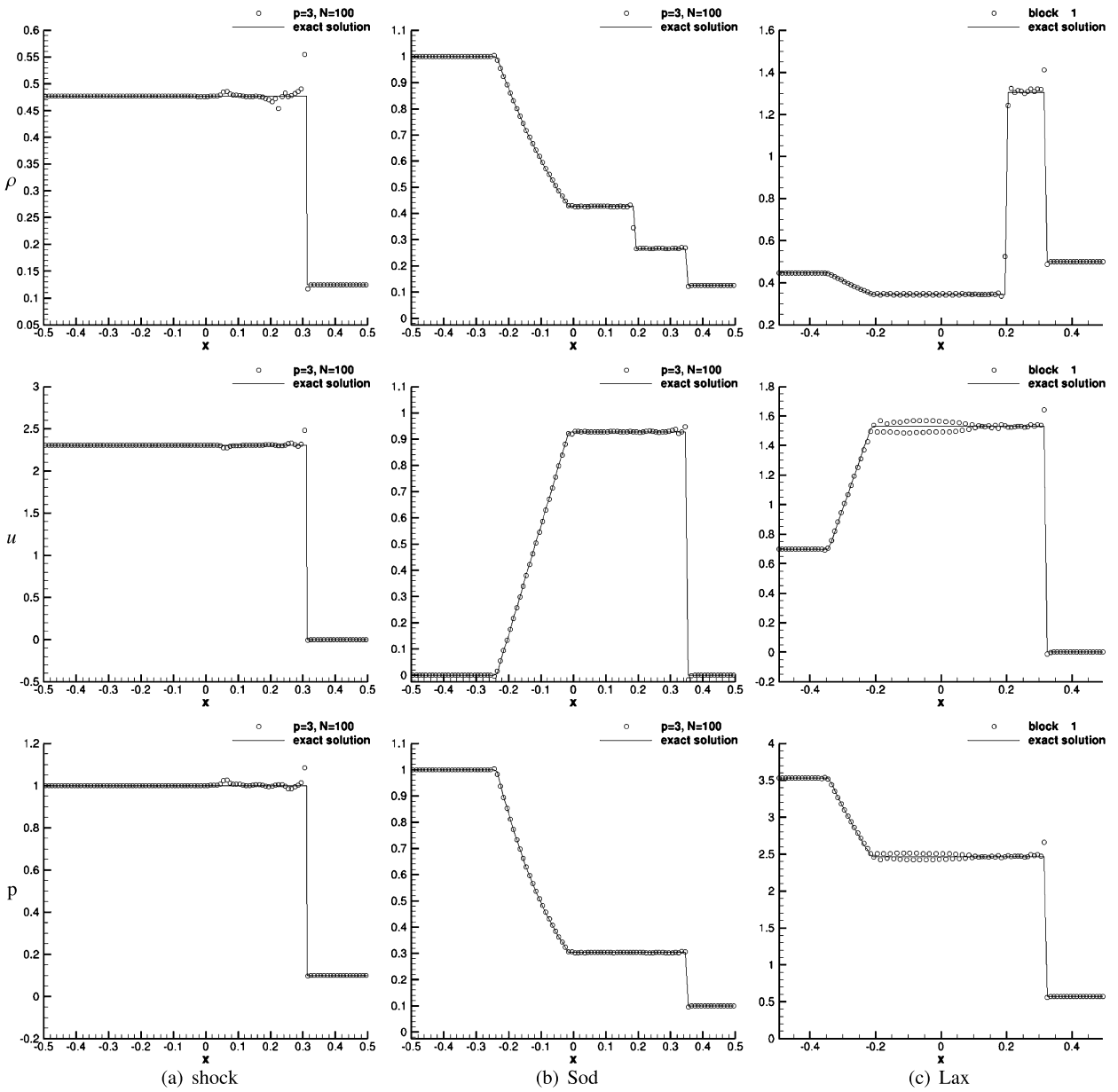


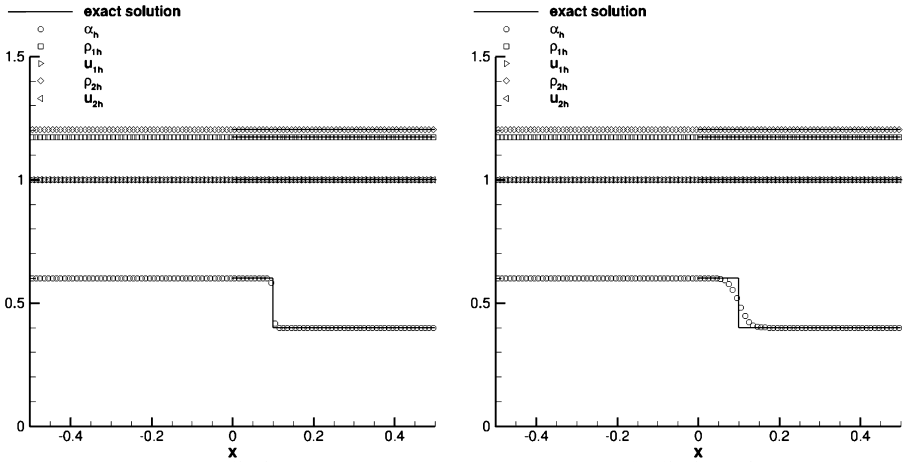
Fig. 5. Euler equations: Riemann problems discretized with a polynomial degree $p = 3$, $N = 100$ cells and entropy stable scheme.

computations. However, spurious oscillations still remain in the numerical solutions in the neighborhood of discontinuities which may be attributed to some of the drawbacks of the present approach: semi-discrete entropy stability; entropy stability for the cell-averaged DGSEM only; stabilization introduced only through numerical fluxes that does not stabilize internal DOFs; positivity of the solution not guaranteed with the Lagrange interpolation polynomials even if nodal values are positive; integration error associated to mass lumping; etc.

Future work will concern the improvement of the limiter to preserve contact discontinuities, the analysis of the well-balanced property, and the extension of the method to the Baer–Nunziato model with general equations of states including the transport equations for partial energies [7].

Appendix A. Entropy conservative fluctuation fluxes

In the following, we provide further examples of entropy conservative numerical fluxes of the form (27) for different nonconservative systems. We recall the definitions of the jump and average operators: $[\![u]\!] := u^+ - u^-$ and $\overline{u} := \frac{u^- + u^+}{2}$.



(a) no limiter (b) limiter (67)

Fig. 6. Isentropic Baer–Nunziato model: advection of a void fraction discontinuity discretized with polynomial degree $p = 3$, $N = 100$ cells and entropy stable scheme.

A.1. Coupled Burgers' equation

The following nonconservative system was first proposed in [8]:

$$\partial_t u + u\partial_x(u+v) = 0, \quad \partial_t v + v\partial_x(u+v) = 0,$$

where we recover the Burgers' equation for the sum $u + v$. Entropy and entropy flux are therefore $\eta(\mathbf{u}) = \frac{(u+v)^2}{2}$ and $q(\mathbf{u}) = \frac{(u+v)^3}{3}$. Entropy conservative fluctuation fluxes of the form (27) may also be derived:

$$\mathbf{D}_{ec}^-(\mathbf{u}^-,\mathbf{u}^+) = \frac{[\![u+v]\!]}{6}\begin{pmatrix} 2u^- + u^+ \\ 2v^- + v^+ \end{pmatrix}, \quad \mathbf{D}_{ec}^+(\mathbf{u}^-,\mathbf{u}^+) = \frac{[\![u+v]\!]}{6}\begin{pmatrix} u^- + 2u^+ \\ v^- + 2v^+ \end{pmatrix},$$

which correspond to the path-conservative and entropy conservative fluxes derived in [12].

A.2. Euler equations in Lagrangian coordinates

The Euler equations in Lagrangian coordinates may be written in nonconservative form:

$$\partial_t \tau - \partial_x u = 0, \quad \partial_t u + \partial_x \mathrm{p} = 0, \quad \partial_t e + \mathrm{p}\partial_x u = 0,$$

with τ the specific volume, u the velocity, e the specific internal energy. The equations are supplemented with a general equation of states for the pressure $\mathrm{p} = \mathrm{p}(\tau, e)$ and admissible solutions satisfy the entropy inequality

$$-\partial_t \mathrm{s} \le 0,$$

with $\mathrm{T}ds = de + \mathrm{p}d\tau$, and T the temperature.

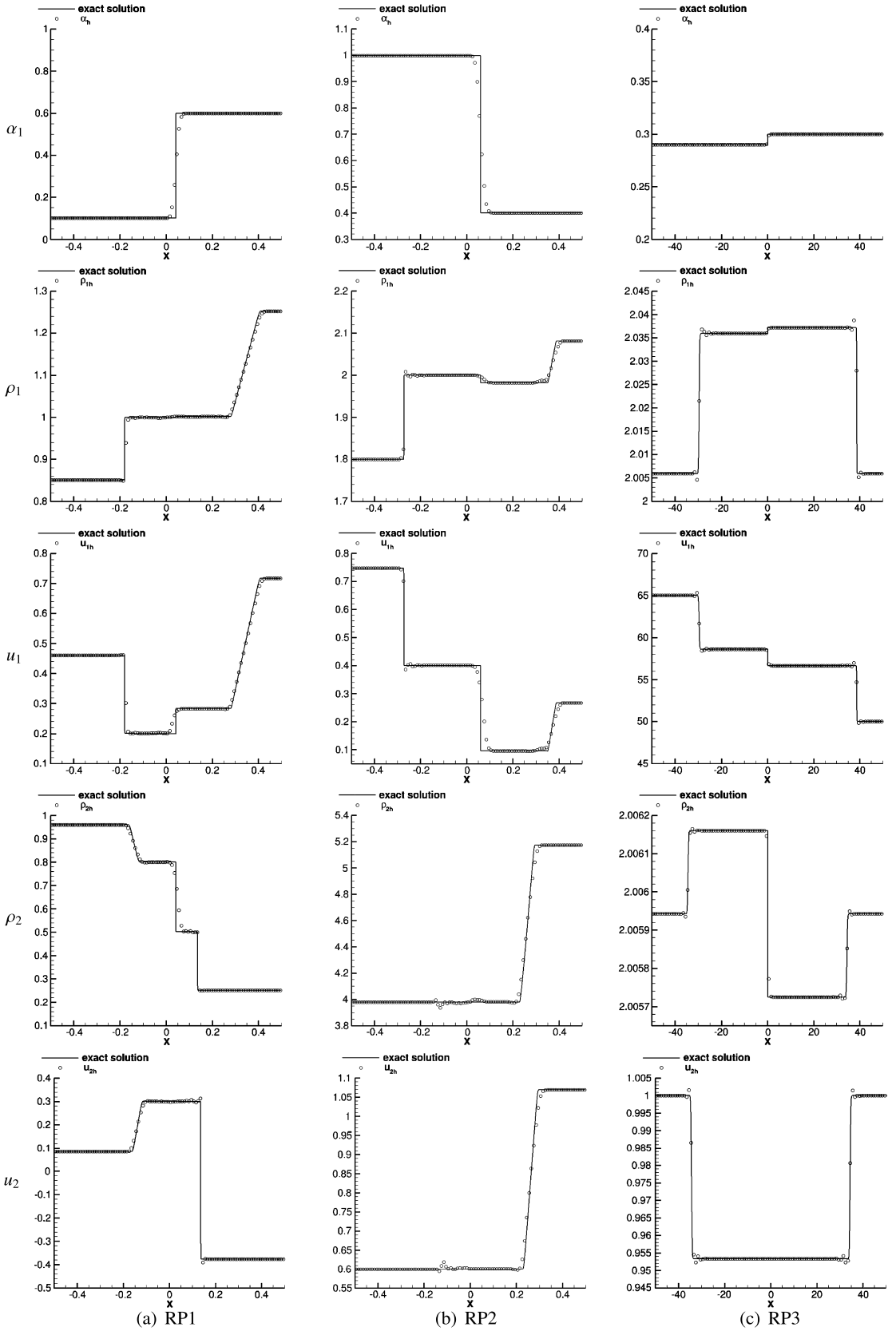
Entropy conservative fluctuation fluxes are

$$\mathbf{D}_{ec}^-(\mathbf{u}^-,\mathbf{u}^+) = \frac{1}{2}\begin{pmatrix} -[\![u]\!] \\ [\![\mathrm{p}]\!] \\ \mathrm{p}^-[\![u]\!] \end{pmatrix}, \quad \mathbf{D}_{ec}^+(\mathbf{u}^-,\mathbf{u}^+) = \frac{1}{2}\begin{pmatrix} -[\![u]\!] \\ [\![\mathrm{p}]\!] \\ \mathrm{p}^+[\![u]\!] \end{pmatrix}.$$

Note that these fluxes are different from the path-conservative Roe-type method with straight-line paths in τ, u and p [4,14,59] where the fluctuation fluxes read

$$\mathbf{D}_{roe}^{\pm}(\mathbf{u}^-,\mathbf{u}^+) = \mathcal{A}(\mathbf{u}^-,\mathbf{u}^+)^{\pm}[\![\mathbf{u}]\!] = \mathbf{A}(\tilde{\mathbf{v}})[\![\mathbf{u}]\!],$$

with $\tilde{\mathbf{v}} = (\overline{\tau}, \overline{u}, \overline{\mathrm{p}})^\top$.



(a) RP1 (b) RP2 (c) RP3

Fig. 7. Isentropic Baer–Nunziato model: Riemann problems discretized with a polynomial degree $p = 3$, $N = 100$ cells and entropy stable scheme.

A.3. Shallow water equations

The Shallow water equations with topography read

$$\partial_t b = 0, \quad \partial_t h + \partial_x(hu) = 0, \quad \partial_t(hu) + \partial_x(hu^2 + \tfrac{1}{2}gh^2) + gh\partial_x b = 0,$$

where h, u, b are the water height, depth-averaged velocity, bottom topography, and g denotes the gravitational acceleration. The entropy and entropy flux are $\eta(\mathbf{u}) = \frac{hu^2+gh^2}{2} + ghb$ and $q(\mathbf{u}) = \frac{hu^3}{2} + ghu(h+b)$.

Entropy conservative fluctuation fluxes are

$$\mathbf{D}_{ec}^-(\mathbf{u}^-,\mathbf{u}^+) = \begin{pmatrix} 0 \\ \overline{h}\overline{u} - h^- u^- \\ \overline{h}\big(\frac{g\overline{h}}{2} + \overline{u}^2\big) - h^-\big(\frac{gh^-}{2} + (u^-)^2\big) + \frac{g\overline{h}}{2}[\![b]\!] \end{pmatrix},$$

$$\mathbf{D}_{ec}^+(\mathbf{u}^-,\mathbf{u}^+) = \begin{pmatrix} 0 \\ h^+u^+ - \overline{h}\overline{u} \\ h^+\big(\frac{gh^+}{2} + (u^+)^2\big) - \overline{h}\big(\frac{g\overline{h}}{2} + \overline{u}^2\big) + \frac{g\overline{h}}{2}[\![b]\!] \end{pmatrix}.$$

Neglecting topography, i.e., $b \equiv 0$, the shallow water equations are in conservative form for the conservative variables $\mathbf{u} = (h, hu)^\top$ and fluxes $\mathbf{f}(\mathbf{u}) = (hu, hu^2 + gh^2/2)^\top$. Using again (32) to construct a symmetric entropy conservative flux, we obtain

$$\mathbf{h}_{ec}(\mathbf{u}^-,\mathbf{u}^+) = \begin{pmatrix} \overline{h}\overline{u} \\ \frac{g\overline{h}^2}{2} + \overline{h}\overline{u}^2 \end{pmatrix},$$

which corresponds the entropy conservative flux derived in [28].

A.4. One-pressure model of spray dynamics

We now consider the one-pressure two-velocity four equations system for modeling the dynamics of a spray of liquid droplets in a gas at thermodynamic equilibrium [49,52]. Let ρ_g be the gas density, $\rho_l > 0$ the constant and uniform liquid density, α the void fraction of the gas, and u_g and u_l the velocities of the gas and liquid phases. The variables obey the following hyperbolic system

$$\begin{aligned} \partial_t(\alpha\rho_g) + \partial_x(\alpha\rho_g u_g) &= 0, \\ \partial_t(\alpha\rho_g u_g) + \partial_x(\alpha_g\rho_g u_g^2) + \alpha\partial_x \mathrm{p} &= 0, \\ \partial_t\big((1-\alpha)\rho_l\big) + \partial_x\big((1-\alpha)\rho_l u_l\big) &= 0, \\ \partial_t\big((1-\alpha)\rho_l u_l\big) + \partial_x\big((1-\alpha)\rho_l u_l^2\big) + (1-\alpha)\partial_x \mathrm{p} + \partial_x\theta &= 0, \end{aligned}$$

over the set of states $\Omega^a = \{\mathbf{u} \in \mathbb{R}^4 : \ \rho_g > 0, 0 < \alpha < 1\}$. The gas pressure $\mathrm{p} = \mathrm{p}(\rho_g)$ satisfies $\mathrm{p}'(\rho_g) > 0$, and $\theta(\alpha) = \theta_0(1-\alpha)^\delta$, with $1 < \delta < 2$, where θ_0 denotes the total pressure of the gas on a droplet. The system satisfies an entropy inequality (3) for the pair

$$\begin{aligned} \eta(\mathbf{u}) &= \alpha\rho_g\Big(\frac{u_g^2}{2} + e(\rho_g)\Big) + (1-\alpha)\rho_l\frac{u_l^2}{2} + \frac{\theta(\alpha)}{\delta-1}, \\ q(\mathbf{u}) &= \alpha\rho_g\Big(\frac{u_g^2}{2} + \mathrm{h}(\rho_g)\Big)u_g + (1-\alpha)\Big(\rho_l\frac{u_l^2}{2} + \mathrm{p}(\rho_g)\Big)u_l + \frac{\delta}{\delta-1}\theta(\alpha)u_l, \end{aligned}$$

where $\rho_g^2 e'(\rho_g) = \mathrm{p}(\rho_g)$ and $\mathrm{h}(\rho_g) = e(\rho_g) + \mathrm{p}(\rho_g)/\rho_g$. It can be checked that the following fluxes are entropy conservative:

$$\mathbf{D}_{ec}^-(\mathbf{u}^-,\mathbf{u}^+) = \begin{pmatrix} \hat{h}_g - \alpha^-\rho_g^- u_g^- \\ \hat{h}_g\overline{u_g} + \overline{\alpha}\,\overline{\mathrm{p}} - \alpha^-(\rho_g^-(u_g^-)^2 + \mathrm{p}^-) - \frac{\mathrm{p}^-}{2}[\![\alpha]\!] \\ \hat{h}_l - (1-\alpha^-)\rho_l u_l^- \\ \hat{h}_l\overline{u_l} + \overline{1-\alpha}\,\overline{\mathrm{p}} - (1-\alpha^-)(\rho_l(u_l^-)^2 + \mathrm{p}^-) + \frac{\mathrm{p}^-}{2}[\![\alpha]\!] + \frac{[\![\theta]\!]}{2} \end{pmatrix},$$

$$\mathbf{D}_{ec}^{+}(\mathbf{u}^{-},\mathbf{u}^{+}) = \begin{pmatrix} \alpha^{+}\rho_g^{+}u_g^{+} - \hat{h}_g \\ \alpha^{+}(\rho_g^{+}(u_g^{+})^2 + \mathrm{p}^{+}) - \hat{h}_g\overline{u_g} - \overline{\alpha}\,\overline{\mathrm{p}} - \frac{\mathrm{p}^{+}}{2}[\![\alpha]\!] \\ (1-\alpha^{+})\rho_l u_l^{+} - \hat{h}_l \\ (1-\alpha^{+})(\rho_l(u_l^{+})^2 + \mathrm{p}^{+}) - \hat{h}_l\overline{u_l} - \overline{1-\alpha}\,\overline{\mathrm{p}} + \frac{\mathrm{p}^{+}}{2}[\![\alpha]\!] + \frac{[\![\theta]\!]}{2} \end{pmatrix},$$

where

$$\hat{h}_g = \begin{cases} \overline{\alpha}\,\overline{u_g}\frac{[\![\mathrm{p}(\rho_g)]\!]}{[\![\mathrm{h}(\rho_g)]\!]} & \text{if } \rho_g^{-} \neq \rho_g^{+}, \\ \overline{\alpha}\,\overline{u_g}\rho_g & \text{if } \rho_g^{-} = \rho_g^{+} = \rho_g, \end{cases}$$

$$\hat{h}_l = \begin{cases} \rho_l\frac{\overline{1-\alpha}\,\overline{u_l}[\![\mathrm{p}(\rho_g)]\!]+\overline{u_l}[\![\theta(\alpha)]\!]}{[\![\mathrm{p}(\rho_g)]\!]+\frac{\delta}{\delta-1}[\![\theta(\alpha)]\!]} & \text{if } \rho_g^{-} \neq \rho_g^{+} \text{ or } \alpha^{-} \neq \alpha^{+}, \\ \rho_l(1-\alpha)\overline{u_l} & \text{if } \rho_g^{-} = \rho_g^{+} = \rho_g \text{ and } \alpha^{-} = \alpha^{+} = \alpha. \end{cases}$$

References

[1] R. Abgrall, How to prevent pressure oscillations in multicomponent flow calculations: a quasi conservative approach, J. Comput. Phys. 125 (1996) 150–160.
[2] R. Abgrall, A general framework to construct schemes satisfying additional conservation relations: application to entropy conservative and entropy dissipative schemes, arXiv:1711.10358 [math.NA], 2018.
[3] R. Abgrall, E. le Mélédo, P. Öffner, On the connection between residual distribution schemes and flux reconstruction, preprint, arXiv:1807.01261 [math.NA], 2018.
[4] R. Abgrall, S. Karni, A comment on the computation of non-conservative products, J. Comput. Phys. 45 (2010) 382–403.
[5] R. Abgrall, H. Kumar, Numerical approximation of a compressible multiphase system, Commun. Comput. Phys. 15 (2014) 1237–1265.
[6] A. Ambroso, C. Chalons, F. Coquel, T. Galié, E. Godlewski, P.-A. Raviart, N. Seguin, The drift-flux asymptotic limit of barotropic two-phase two-pressure models, Commun. Math. Sci. 6 (2008) 521–529.
[7] M.R. Baer, J.W. Nunziato, A two-phase mixture theory for the deflagration-to-detonation transition (DDT) in reactive granular materials, Int. J. Multiphase Flow 12 (1986) 861–889.
[8] C. Berthon, Nonlinear scheme for approximating a non-conservative hyperbolic system, C. R. Math. Acad. Sci. Paris 335 (2002) 1069–1072.
[9] C. Berthon, F. Coquel, P.G. LeFloch, Why many theories of shock waves are necessary: kinetic relations for non-conservative systems, Proc. R. Soc. Edinb. 142 (2012) 1–37.
[10] M. Bohm, A.R. Winters, G.J. Gassner, D. Derigs, F. Hindenlang, J. Saur, An entropy stable nodal discontinuous Galerkin method for the resistive MHD equations, part I: theory and numerical verification, J. Comput. Phys. (2019), https://doi.org/10.1016/j.jcp.2018.06.027, in press.
[11] M.H. Carpenter, T.C. Fisher, E.J. Nielsen, S.H. Frankel, Entropy stable spectral collocation schemes for the Navier–Stokes equations: discontinuous interfaces, SIAM J. Sci. Comput. 36 (2014) B835–B867.
[12] M.J. Castro, U.S. Fjordholm, S. Mishra, C. Parès, Entropy conservative and entropy stable schemes for nonconservative hyperbolic systems, SIAM J. Numer. Anal. 51 (2013) 1371–1391.
[13] M.J. Castro, P.G. LeFloch, M.L. Munõz-Ruiz, C. Parès, Why many theories of shock waves are necessary: convergence error in formally path-consistent schemes, J. Comput. Phys. 227 (2008) 8107–8129.
[14] Ch. Chalons, F. Coquel, A new comment on the computation of non-conservative products using Roe-type path conservative schemes, J. Comput. Phys. 335 (2017) 592–604.
[15] P. Chandrashekar, C. Klingenberg, Entropy stable finite volume scheme for ideal compressible MHD on 2-D Cartesian meshes, SIAM J. Numer. Anal. 54 (2016) 1313–1340.
[16] T. Chen, C.-W. Shu, Entropy stable high order discontinuous Galerkin methods with suitable quadrature rules for hyperbolic conservation laws, J. Comput. Phys. 345 (2017) 427–461.
[17] F. Coquel, T. Gallouët, J.-M. Hérard, N. Seguin, Closure laws for a two-fluid two-pressure model, C. R. Acad. Sci. Paris 334 (2002) 927–932.
[18] F. Coquel, J.-M. Hérard, K. Saleh, N. Seguin, A robust entropy-satisfying finite volume scheme for the isentropic Baer–Nunziato model, ESAIM: Math. Model. and Numer. Analysis (M2AN) 48 (2013) 165–206.
[19] F. Coquel, C. Marmignon, P. Rai, F. Renac, Adjoint approximation of nonlinear hyperbolic systems with non-conservative products, in: XVII International Conference on Hyperbolic Problems, Theory, Numerics, Applications, University Park, USA, 2018.
[20] G. Dal Maso, P.G. LeFloch, F. Murat, Definition and weak stability of nonconservative products, J. Math. Pures Appl. 74 (1995) 483–548.
[21] B. Després, Entropy inequality for high order discontinuous Galerkin approximation of Euler equations, in: VII Conference on Hyperbolic Problems, ETHZ-Zurich, 1998.
[22] B. Després, Discontinuous Galerkin method for the numerical solution of Euler equations in axisymmetric geometry, in: B. Cockburn, G.E. Karniadakis, C.-W. Shu (Eds.), Discontinuous Galerkin Methods: Theory, Computation and Applications, in: Lecture Notes in Computational Science and Engineering, vol. 11, Springer-Verlag, 2000, pp. 315–320.
[23] M. Dumbser, W. Boscheri, High-order unstructured Lagrangian one-step WENO finite volume schemes for non-conservative hyperbolic systems: applications to compressible multi-phase flows, Comput. Fluids 86 (2013) 405–432.
[24] M. Dumbser, V. Casulli, A staggered semi-implicit spectral discontinuous Galerkin scheme for the shallow water equations, Appl. Math. Comput. 219 (2013) 8057–8077.
[25] M. Dumbser, A. Hidalgo, M. Castro, C. Parés, E. Toro, FORCE schemes on unstructured meshes II: non-conservative hyperbolic systems, Comput. Methods Appl. Mech. Eng. 199 (2010) 625–647.
[26] M. Dumbser, R. Loubère, A simple robust and accurate a posteriori sub-cell finite volume limiter for the discontinuous Galerkin method on unstructured meshes, J. Comput. Phys. 319 (2016) 163–199.
[27] T.C. Fisher, M.H. Carpenter, High-order entropy stable finite difference schemes for nonlinear conservation laws: finite domains, J. Comput. Phys. 252 (2013) 518–557.
[28] U.S. Fjordholm, S. Mishra, E. Tadmor, Arbitrarily high-order accurate entropy stable essentially nonoscillatory schemes for systems of conservation laws, SIAM J. Numer. Anal. 50 (2012) 544–573.

[29] E. Franquet, V. Perrier, Runge–Kutta discontinuous Galerkin method for the approximation of Baer and Nunziato type multiphase models, J. Comput. Phys. 231 (2012) 4096–4141.
[30] E. Franquet, V. Perrier, Runge–Kutta discontinuous Galerkin method for reactive multiphase flows, Comput. Fluids 83 (2013) 157–163.
[31] F. Fraysse, C. Redondo, G. Rubio, E. Valero, Upwind methods for the Baer–Nunziato equations and higher-order reconstruction using artificial viscosity, J. Comput. Phys. 326 (2016) 805–827.
[32] G.J. Gassner, A Skew-symmetric discontinuous Galerkin spectral element discretization and its relation to SBP-SAT finite difference methods, SIAM J. Sci. Comput. 35 (2013) A1233–A1253.
[33] G.J. Gassner, A.R. Winters, D.A. Kopriva, A well balanced and entropy conservative discontinuous Galerkin spectral element method for the shallow water equations, Appl. Math. Comput. 272 (2016) 291–308.
[34] G.J. Gassner, A.R. Winters, D.A. Kopriva, Split form nodal discontinuous Galerkin schemes with summation-by-parts property for the compressible Euler equations, J. Comput. Phys. 327 (2016) 39–66.
[35] A. Hiltebrand, S. Mishra, Entropy stable shock capturing space–time discontinuous Galerkin schemes for systems of conservation laws, Numer. Math. 126 (2014) 103–151.
[36] M.T. Henry de Frahan, S. Varadan, E. Johnsen, A new limiting procedure for discontinuous Galerkin methods applied to compressible multiphase flows with shocks and interfaces, J. Comput. Phys. 280 (2015) 89–509.
[37] F. Ismail, P.L. Roe, Affordable, entropy-consistent Euler flux functions, II: entropy production at shocks, J. Comput. Phys. 228 (2009) 5410–5436.
[38] G. Jiang, C.W. Shu, On a cell entropy inequality for discontinuous Galerkin methods, Math. Comput. 62 (1994) 531–538.
[39] D.A. Kopriva, G. Gassner, On the quadrature and weak form choices in collocation type discontinuous Galerkin spectral element methods, J. Sci. Comput. 44 (2010) 136–155.
[40] Ph. Le Floch, Shock waves for nonlinear hyperbolic systems in nonconservative form, Preprint 593, Inst. of Math, and Its Applications, Univ. of Minnesota, Minneapolis, October 1989.
[41] Y. Liu, C.-W. Shu, M. Zhang, Entropy stable high order discontinuous Galerkin methods for ideal compressible MHD on structured meshes, J. Comput. Phys. 354 (2018) 163–178.
[42] S.T. Munkejord, Comparison of Roe-type methods for solving the two-fluid model with and without pressure relaxation, Comput. Fluids 36 (2007) 1061–1080.
[43] C. Parès, Numerical methods for non-conservative hyperbolic systems: a theoretical framework, SIAM J. Numer. Anal. 44 (2006) 300–321.
[44] B. Perthame, C.-W. Shu, On positivity preserving finite volume schemes for Euler equations, Numer. Math. 73 (1996) 119–130.
[45] H. Ranocha, Shallow water equations: split-form, entropy stable, well-balanced, and positivity preserving numerical methods, GEM-Int. J. Geomath. 8 (2017) 85–133.
[46] F. Renac, A robust high-order Lagrange-projection like scheme with large time steps for the isentropic Euler equations, Numer. Math. 135 (2017) 493–519.
[47] F. Renac, A robust high-order discontinuous Galerkin method with large time steps for the compressible Euler equations, Commun. Math. Sci. 15 (2017) 813–837.
[48] S. Rhebergen, O. Bokhove, J.J.W. van der Vegt, Discontinuous Galerkin finite element methods for hyperbolic nonconservative partial differential equations, J. Comput. Phys. 227 (2008) 1887–1922.
[49] L. Sainsaulieu, Ondes progressives solutions de systèmes convectifs–diffusifs et systèmes hyperboliques non conservatifs, C. R. Math. Acad. Sci. Paris 312 (1991) 491–494.
[50] D. Serre, Domaines invariants pour les systèmes hyperboliques de lois de conservation, J. Differential Equations 69 (1987) 46–62.
[51] C.-W. Shu, S. Osher, Efficient implementation of essentially non-oscillatory shock-capturing schemes, J. Comput. Phys. 77 (1988) 439–471.
[52] H.B. Stewart, B. Wendroff, Two-phase flow: models and methods, J. Comput. Phys. 56 (1984) 363–409.
[53] E. Tadmor, Skew-selfadjoint form for systems of conservation law, J. Math. Anal. Appl. 103 (1984) 428–442.
[54] E. Tadmor, A minimum entropy principle in the gas dynamics equations, Appl. Numer. Math. 2 (1986) 211–219.
[55] E. Tadmor, The numerical viscosity of entropy stable schemes for systems of conservation laws. I, Math. Comput. 49 (1987) 91–103.
[56] P.A. Tassi, S. Rhebergen, C.A. Vionnet, O. Bokhove, A discontinuous Galerkin finite element model for river bed evolution under shallow flows, Comput. Methods Appl. Mech. Engrg. 197 (2008) 2930–2947.
[57] S.A. Tokareva, E.F. Toro, HLLC-type Riemann solver for the Baer–Nunziato equations of compressible two-phase flow, J. Comput. Phys. 229 (2010) 3573–3604.
[58] S.A. Tokareva, E.F. Toro, A flux splitting method for the Baer–Nunziato equations of compressible two-phase flow, J. Comput. Phys. 323 (2016) 45–74.
[59] I. Toumi, A weak formulation of Roe's approximate Riemann solver, J. Comput. Phys. 102 (1992) 360–373.
[60] A.L. Volpert, The space BV and quasilinear equations, Math. USSR Sbornik 73 (1967) 225–267.
[61] X. Zhang, C.-W. Shu, On maximum-principle-satisfying high order schemes for scalar conservation laws, J. Comput. Phys. 229 (2010) 3091–3120.
[62] X. Zhang, C.-W. Shu, On positivity-preserving high order discontinuous Galerkin schemes for compressible Euler equations on rectangular meshes, J. Comput. Phys. 229 (2010) 8918–8934.
[63] J.S.B. van Zwieten, B. Sanderse, M.H.W. Hendrix, C. Vuik, R.A.W.M. Henkes, Efficient simulation of one-dimensional two-phase flow with a high-order h-adaptive space–time discontinuous Galerkin method, Comput. Fluids 156 (2017) 34–47.